UNIVERSITY OF BIRMINGHAM

University of Birmingham Research at Birmingham

Dehydrogenation and rehydrogenation of a 0.62LiBH$_4$-0.38NaBH$_4$ mixture with nano-sized Ni

Liu, Yinzhe; Heere, Michael; Contreras, Luis; Paterakis, Christos; Sørby, Magnus; Hauback, Bjørn; Book, David

[Link to publication on Research at Birmingham portal](#)

Dehydrogenation and rehydrogenation of a $0.62LiBH_4$-$0.38NaBH_4$ mixture with nano-sized Ni

Yinzhe Liu[a], Michael Heere[b,c], Luis Contreras Vasquez[a], Christos Paterakis[a], Magnus H. Sørby[b], Bjørn C. Hauback[b], David Book[a]

a School of Metallurgy and Materials, University of Birmingham, Birmingham, B15 2TT, UK

b Physics Department, Institute for Energy Technology, Kjeller, NO-2027, Norway

c Institute for Applied Materials (IAM), Karlsruhe Institute of Technology (KIT), Eggenstein–Leopoldshafen, D–76344, Germany

YXL454@student.bham.ac.uk

Abstract

The dehydrogenation reaction pathways of a $0.91(0.62LiBH_4$-$0.38NaBH_4)$-$0.09Ni$ mixture in the temperature range of 25-650 °C in flowing Ar and the cycling stability in H_2 are presented. No H_2 is released immediately after melting at 225 °C. The major dehydrogenation occurs above 350 °C. Adding nano-sized Ni reduces the dehydrogenation peak temperatures by 20-25 °C, leading to three decomposition steps where Ni_4B_3 and $Li_{1.2}Ni_{2.5}B_2$ are found in the major dehydrogenation products for the 1st and the 3rd step; whilst the Ni-free mixture decomposes through a two-step decomposition pathway. A total of 8.1 wt.% of hydrogen release from the $0.91(0.62LiBH_4$-$0.38NaBH_4)$-$0.09Ni$ mixture is achieved at 650 °C in Ar. This mixture has a poor hydrogen cycling stability as its reversible hydrogen content decreases from 5.1 wt.% to 1.1 wt.% and 0.6 wt.% during three complete desorption-absorption-cycles. However, the addition of nano-sized Ni facilitates the reformation of $LiBH_4$.

Keywords

Hydrogen storage; Nanomaterial; Eutectic borohydrides; Dehydrogenation; Rehydrogenation; Reaction pathways

1 Introduction

Due to its high energy content, hydrogen is considered one of the most promising energy vectors for use in establishing sustainable energy systems [1,2]. One of the main challenges for the use of hydrogen as a fuel is the safe and efficient storage of hydrogen [3]. Hydrogen can be stored in several different ways, among which the solid-state storage approach has received extensive attention [4–7].

Metal borohydrides, such as $LiBH_4$ or $Mg(BH_4)_2$, chemically store the hydrogen atoms by covalently bonding hydrogen to boron in the complex anion $[BH_4]^-$. Such compounds have been considered as promising solid-state hydrogen storage media since 2003, due to their high volumetric hydrogen content and low operating pressures (<12 bar) [5,8–14]. For instance, the volumetric hydrogen density of $LiBH_4$ is 121 kg H_2 m^{-3} [8], which is about four times higher than the 40 kg H_2 m^{-3} for gaseous H_2 compressed at 700 bar [15]. However, the hydrogen release and uptake properties of metal borohydrides are often hindered by poor thermodynamics (i.e. high temperatures are required) and sluggish kinetics, which has prevented their use as reversible hydrogen stores [5].

One of the potential approaches to decrease the hydrogen sorption temperatures of borohydrides is to form low-melting-point borohydride mixtures, such as $LiBH_4$-$NaBH_4$, $LiBH_4$-KBH_4, $LiBH_4$-$Mg(BH_4)_2$, $LiBH_4$-$Ca(BH_4)_2$ and $NaBH_4$-KBH_4 [16–22]. These mixtures are often called eutectic borohydrides and have lower fusion temperatures than their pure constituents, leading to dehydrogenation at relatively low temperatures through kinetic effects [11]. In fact, the nature of molten salts is critical in utilizing H_2 release from borohydrides, especially from alkali-metal borohydrides that often melt before their major H_2 desorption begin

[11]. In addition, the dehydrogenation of borohydrides from the liquid rather than the solid state may lead to less unwanted phases in the reaction products, such as $[B_{10}H_{10}]^{2-}$ and $[B_{12}H_{12}]^{2-}$ phases [23]. Since metal dodecaborates act as boron sinks that hinder the rehydrogenation of decomposed borohydrides [24,25], the formation of such compounds is not favorable and needs to be avoided in solid-state hydrogen storage systems. Moreover, the low melting point is beneficial for the nanoconfinement-by-infiltration approach, in which molten borohydrides are infiltrated into a porous material to reduce the decomposition temperature as well as to improve the reversibility [26–32].

The eutectic $LiBH_4$-$NaBH_4$ mixture has received attention owing to its relatively low cost among known eutectic borohydride mixtures and a high theoretical gravimetric hydrogen storage capacity of approximately 15 wt.% [17]. According to experimental measurements and theoretical calculations, two eutectic compositions have been proposed in the past: $0.62LiBH_4$-$0.38NaBH_4$ [17,28] and $0.71LiBH_4$-$0.29NaBH_4$ [33]. The melting of this kind of mixtures occurs at around 216-225 °C [28,33], which is about 60 °C lower than that of $LiBH_4$ [34] and about 280 °C lower than that of $NaBH_4$ [35,36]. The dehydrogenation of $0.62LiBH_4$-$0.38NaBH_4$ mixture starts at 287 °C with a total of 10.8 wt.% hydrogen release upon heating to 650 °C in Ar [37]. In general, the decomposition of borohydrides is complex and usually involves the formation of a series of intermediate phases, as a function of temperature and pressure [38–41]. Under an Ar atmosphere, the dehydrogenation pathways of the $0.62LiBH_4$-$0.38NaBH_4$ mixture are mainly accompanied by the precipitation of LiH, $Li_2B_{12}H_{12}$ and B from 287 °C to 520 °C and the formation of Na and B from 520 °C to 650 °C [37]. These high dehydrogenation temperatures are indeed above the US DOE (department of energy) target of on-board H_2 storage for light-duty vehicles [42] and therefore need to be further reduced with the help of a detailed understanding of the dehydrogenation pathways.

Many attempts to tailor the temperature required for dehydrogenation and to improve the cycling stability of borohydrides have been made, such as adding additives/catalysts [9,19,43–47], forming reactive hydride composites [48–55]

and confining into nano-porous scaffolds [56–59]. Furthermore, adding Ni to LiBH$_4$ forms an interesting LiBH$_4$-Ni system, which has received attention due to the low dehydrogenation enthalpy values (18-34 kJ mol^{-1} H$_2$) of the possible chemical reactions (Equation 1-3), generating nickel borides (i.e. N$_4$B$_3$, Ni$_2$B, Ni$_3$B) [60], which have been described as valuable additives [60–62]. The addition of 25 wt.% nano-sized Ni to LiBH$_4$ reduces the dehydrogenation peak temperature by 50 °C, and improves the reversible hydrogen content from 4.3 wt.% for Ni-free sample to 10.8 wt.% as a consequence of the effect of the Ni$_4$B$_3$ [60].

$$6LiBH_4 + 8Ni = 2Ni_4B_3 + 6LiH + 9H_2 \qquad\qquad \textbf{Equation 1}$$

$$2LiBH_4 + 4Ni = 2Ni_2B + 2LiH + 3H_2 \qquad\qquad \textbf{Equation 2}$$

$$2LiBH_4 + 6Ni = 2Ni_3B + 2LiH + 3H_2 \qquad\qquad \textbf{Equation 3}$$
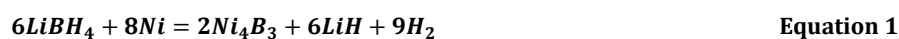
Thus, to reduce the dehydrogenation temperature of the 0.62LiBH$_4$-0.38NaBH$_4$ mixture, this work used 18 wt.% (9 mol%) nano-sized Ni particles as additive. In addition, the modified decomposition pathways were studied by determining the phases and the structural evolution as a function of temperature, using a series of samples heat-treated at selected temperatures through a combination of experimental techniques, i.e. powder X-ray diffraction (PXD), Raman spectroscopy, Fourier Transform infrared spectroscopy (FTIR), Thermogravimetry differential scanning calorimetry (TG-DSC) and temperature programmed desorption – mass spectrometry (TPD-MS). The rehydrogenation of this LiBH$_4$-NaBH$_4$-Ni mixture was also investigated using a Sieverts type apparatus.

2 Materials and Methods

2.1 Synthesis

LiBH$_4$ (≥ 95.0%), NaBH$_4$ (≥ 99.99%) and nano-sized Ni powder (100 nm, ≥ 99.9%) were received from Sigma-Aldrich, stored and handled solely in an Ar glovebox.

The 0.62LiBH$_4$-0.38NaBH$_4$ and 0.91(0.62LiBH$_4$-0.38NaBH$_4$)-0.09Ni mixtures were prepared using a Retsch PM 400 planetary ball mill in 1 bar Ar for 10 h (in total) at 175 rpm. The ball milling process used 250 mL stainless steel milling pots and 13 mm (diameter) stainless steel balls. The ball-to-sample mass ratio was 66:1. To avoid sample overheating during milling, this process was set to rest for 5 min in between every 5 min of operation.

The milled samples were heat-treated by heating at 2 °C min^{-1} in Ar (flowing at 160 mL min^{-1}) to different targets temperatures: 250, 468, 515, 586 and 650 °C. These samples were cooled to room temperature (RT) before further characterization.

2.2 Characterization

2.2.1 Powder X-ray diffraction

Powder X-ray diffraction (PXD) measurements were performed using a Bruker D8 Advance X-Ray Diffractometer with Cu K$_\alpha$ radiation (λ = 1.5418 Å). Samples were loaded and sealed inside a PMMA airtight dome-shaped sample holder inside an Ar glovebox, before transfer to the PXD. The surface of sample was flattened and smoothed to ensure a well-defined geometry. The measurements were performed in the range 2θ = 5–90° at a scanning rate of 2° min^{-1} using a 9 position multi-changer stage. In case of relatively small amount of powder samples, these samples were loaded into rotating glass capillaries (inner diameter = 0.5 mm) and sealed with silicone grease, then measured in 10-70° 2θ at a scanning rate of 1° min^{-1}.

Phase identification from the PXD patterns was performed with EVA software and the PDF-2 database [63]. Quantitative Phase Analysis (QPA) was performed with the Rietveld method using TOPAS-Academic [64] and jEdit software. Published Crystallographic Information Files (*.cif) from the Inorganic Crystal Systems Database [65] for each compound were used for performing the refinements.

2.2.2 Raman/FTIR Spectroscopy

Raman spectroscopy measurements were performed using a Renishaw inVia Reflex Raman spectrometer with a confocal microscope (equipped with a 20x objective). The laser and grating system used were 488 nm (30 mW) and 2400 l mm^{-1}, respectively. About 5-10 mg of sample was loaded in an aluminium crucible, which was placed and sealed in the INSTEC HCS621V cell. Samples were measured in 1 bar Ar. The obtained vibrational modes were analyzed using Renishaw Wire 4.0 [66] and compared with literature data for assignments.

Fourier Transform infrared spectroscopy (FTIR) measurements were carried out inertly using a BRUKER Alpha Platinum-ATR spectrometer. The instrument was placed inside an Ar glove box. A small amount of sample ($\sim$ 2 mg) was placed directly on a diamond disc equipped on the infrared source and then compressed by a one-finger clamp for obtaining intensive signals. The spectra were collected over a wide wavenumber range from 400 to 4000 cm^{-1} with a resolution of 2 cm^{-1} at RT. In general, measurements including 32 scans were averaged for each spectrum and the background. The obtained vibrational results were compared with literature data for assignments.

2.2.3 Thermal Analysis

Thermal properties were investigated using a Netzsch STA 449 F3 Jupiter® Thermogravimetry DSC (TG-DSC). Approximately 1 mg of sample was loaded in an Al crucible and sealed with a lid using mechanical press inside an Ar glovebox. The samples needed to be transferred outside the glovebox for loading onto the TG-DSC, and thus have been exposed to air for a few seconds. The exact amount of sample was weighed out using the balance system equipped on the TG-DSC. The sample was heated at 5 °C min^{-1} in Ar (flowing at 70 mL min^{-1}) from 50 to 250 °C.

2.2.4 Temperature Programmed Desorption

An in–house manufactured Temperature Programmed Desorption (TPD) apparatus connected to a Thermo ProLab Mass Spectrometry (MS) was used to

test the H_2 desorption properties. Around 20 mg powder was loaded into a stainless steel tube and sealed in a T-shape sample holder before being transferred and attached to the TPD frame. Samples were heated at 2 °C min^{-1} in Ar flowing at 160 mL min^{-1} from 50 to 650 °C. The amount of H_2 released from the sample was interpreted using the same method as explained in Ref. [37].

2.2.5 Recombination

A Sieverts type apparatus [67] was used to dehydrogenate and rehydrogenate samples by subjecting them to suitable condition combinations. Approximately 300 mg of sample was loaded into the bottom of the reactor in an Ar glovebox to test the reversible H_2 capacity. The reactor was then sealed, transferred and attached to the Sieverts apparatus. The reaction conditions were: 500 °C, 1 bar H_2 and 10 h for desorption; and 400 °C, 130 bar H_2 and 12 h for absorption.

3 Results and Discussion

3.1 Characterization of as-milled mixture

The nano-sized Ni ($\sim$ 100 nm) was mixed with $LiBH_4$ and $NaBH_4$ by ball milling. The PXD pattern of the as-milled $LiBH_4$-$NaBH_4$-Ni presented in Figure 1 shows Bragg peaks for $LiBH_4$, $NaBH_4$, Ni and NiO phases, suggesting no reaction between the parent borohydrides and additive has occurred during the milling process. The QPA refinement (Figure B. 1 in Supporting Information) suggests the following composition: 40.1(7) wt.% of $LiBH_4$, 42.1(5) wt.% of $NaBH_4$, 16.5(3) wt.% of Ni and 1.3(3) wt.% of NiO, respectively. This small amount of NiO, which was present as a minor impurity phase in the as-received nano-Ni (6 wt%, see Figure A. 1 in Supporting Information), is neglected for simplicity in phase composition reported below. The refined composition of the as-milled sample is $0.91(0.62LiBH_4$-$0.38NaBH_4)$-$0.09Ni$ and is in the following noted as LiNa-Ni. Due to the addition of nano-sized Ni, the nominal phase composition of LiNa-Ni is different from that of $0.62LiBH_4$-$0.38NaBH_4$. However, the molar ratios of $LiBH_4$ to $NaBH_4$ for these two mixtures are identical.
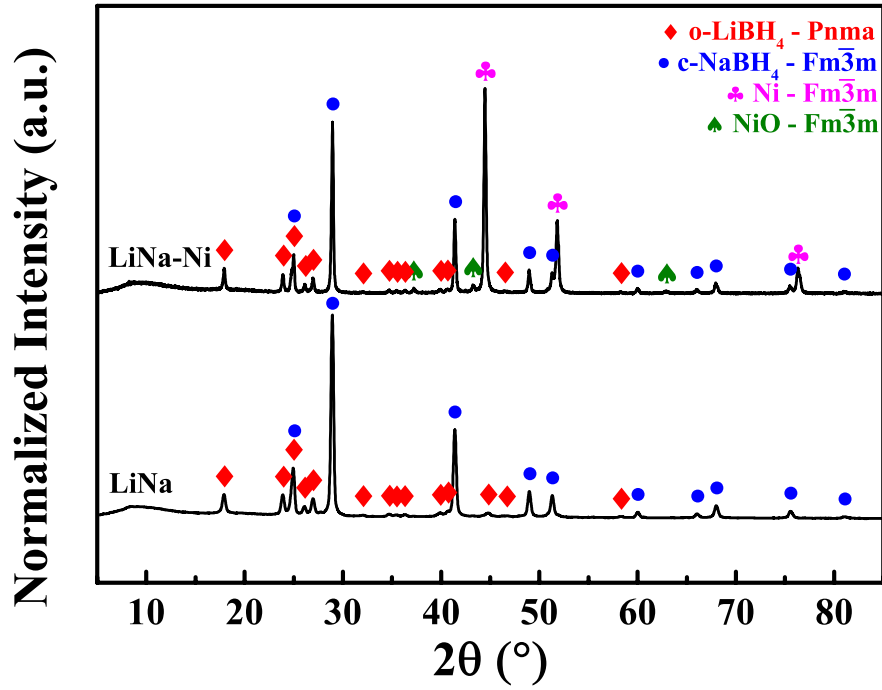
Figure 1 RT PXD (Cu K$_\alpha$, λ = 1.5418 Å) pattern for the as-milled 0.91(0.62LiBH$_4$-0.38NaBH$_4$)-0.09Ni (LiNa-Ni) mixture compared with that for the as-milled 0.62LiBH$_4$-0.38NaBH$_4$ (LiNa) mixture.

In previous work [37], the changes of unit cell volumes of LiBH$_4$ (enlargement) and NaBH$_4$ (shrinkage) components in the as-milled 0.62LiBH$_4$-0.38NaBH$_4$ mixture (noted as LiNa) have been linked to the formation of solid solutions, Li(Na)BH$_4$ and Na(Li)BH$_4$. However, in this work the addition of nano-sized Ni enlarges the refined unit cell volumes for the LiBH$_4$ and NaBH$_4$ constituents in the LiNa-Ni mixture. These values are both larger than that for the LiBH$_4$ and NaBH$_4$ constituents in the LiNa mixture and for as-milled LiBH$_4$ and NaBH$_4$ as shown below:

	LiBH$_4$ in LiNa-Ni		LiBH$_4$ in LiNa [37]		LiBH$_4$ [37]
cell volume [Å^3]	219.71 ± 0.08	>	217.03 ± 0.08	>=	216.84 ± 0.10

	NaBH$_4$ in LiNa-Ni		NaBH$_4$ [37,68]		NaBH$_4$ in LiNa [37]
cell volume [Å^3]	236.91 ± 0.11	>	234.78 ± 0.13	>	234.06 ± 0.022

These increases may be related to the insertion of Ni as interstitials but there is no direct evidence. Furthermore, a systematic error due to different instrument setups / calibration setups cannot be neglected. Thus, it is suggested that the changes in the unit cell volumes cannot be regarded as an indicator for the formation of a solid solution in LiNa-Ni mixture.

Raman and FTIR spectra of LiNa-Ni are shown in Figure 2. The vibrations of B-H stretching and bending modes resemble those of $LiBH_4$ and $NaBH_4$ phases [69–72]. The observed wavenumbers are in good agreement with the Ni-free sample (Table B. 2 and Table B. 3 in Supporting Information) [37]. The measured wavenumbers of the total symmetric stretching mode (ν_1) for $NaBH_4$ in the as-milled LiNa-Ni and LiNa mixtures are found to be 2323 cm^{-1} and 2324 cm^{-1}, respectively. These wavenumbers are 7-8 cm^{-1} lower than the 2331 cm^{-1} measured for as-milled pure $NaBH_4$, suggesting again the volume expansion via an increase in B-H bond length according to Badger's rule [73,74]. This expansion was proposed due to the substitution of Li^+ into $NaBH_4$ [37], suggesting the formation of a $Na(Li)BH_4$ solid solution in the as-milled LiNa-Ni mixture. However, no shift in wavenumbers has been found for the $LiBH_4$ peaks, possibly due to the limited solubility of Na^+ in orthorhombic $LiBH_4$ (o-$LiBH_4$) [33].
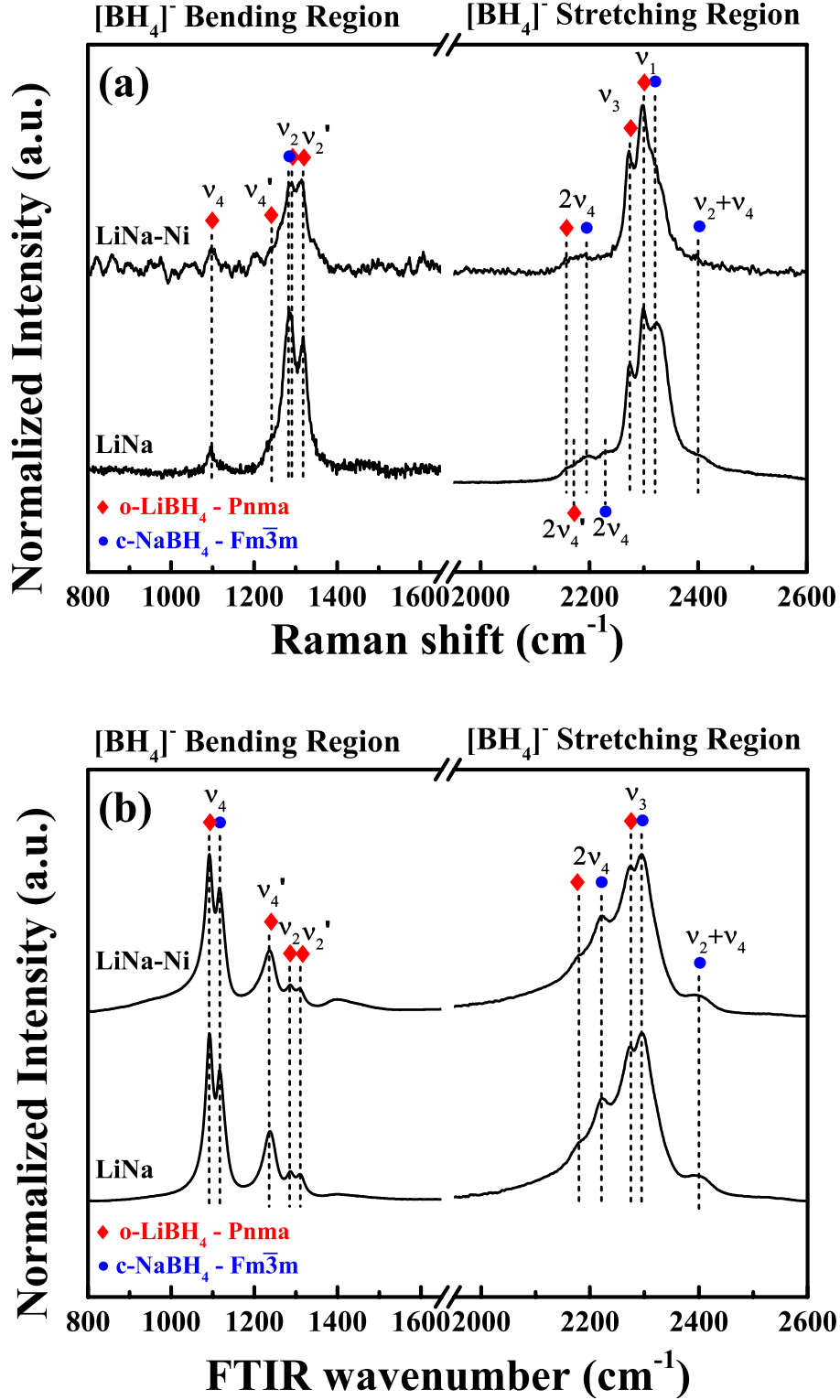
Figure 2 RT Raman (488 nm laser, 2400 l/mm grating system) and FTIR spectra for the as-milled 0.91(0.62LiBH₄-0.38NaBH₄)-0.09Ni (LiNa-Ni) mixture compared with that of as-milled 0.62LiBH₄-0.38NaBH₄ (LiNa) mixture. For better comparisons, the spectra at different regions are normalized to the most intensive peak in the region. Dashed lines are added as a guide for the eye. Due to the high fluorescence effect occurred in the as-milled LiNa-Ni mixture, it has a relatively larger signal to noise ratio in the Raman data than that of the Ni-free sample.

3.2 Melting Behavior

Figure 3 shows the DSC results of as-milled LiNa-Ni mixture compared with the Ni-free mixture.
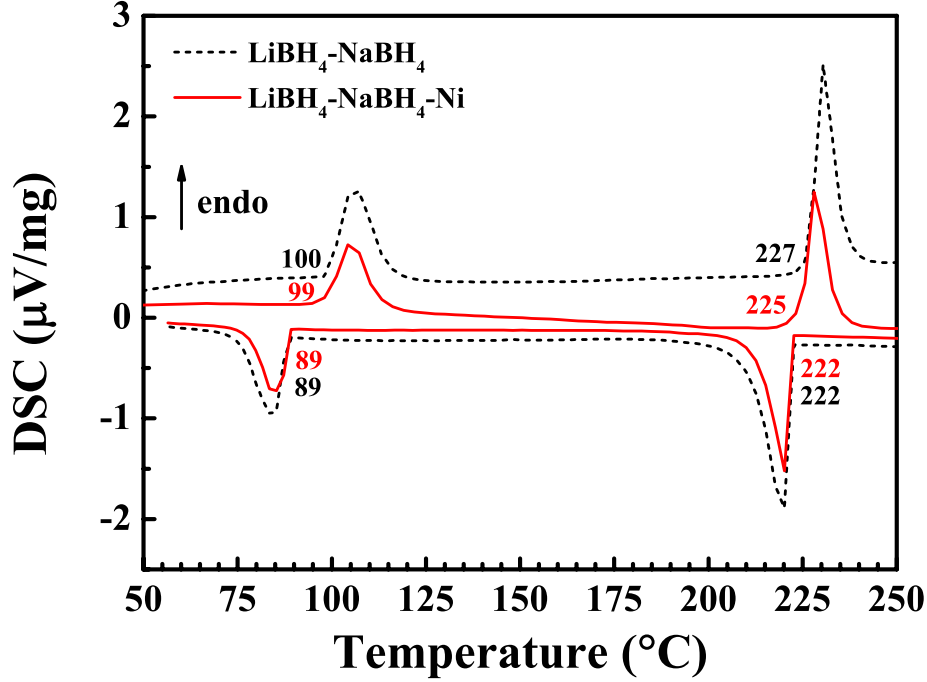

Figure 3 DSC patterns of as-milled 0.91(0.62LiBH₄-0.38NaBH₄)-0.09Ni mixture (red solid curve), compared with the as-milled 0.62LiBH₄-0.38NaBH₄ mixture (black dash curve). Samples were heated from 50 to 250 °C at 5 °C min⁻¹ and then cooled to RT at the same rate in Ar flowing at 70 mL min⁻¹.

The orthorhombic to hexagonal phase transition of $LiBH_4$ in the LiNa-Ni mixture occurs at an onset temperature of 99 ± 1 °C during heating. This is in agreement with the Ni-free sample within the standard deviation, and about 15 °C lower than the common phase transition temperature of $LiBH_4$ (~115 °C) [37]. This temperature reduction was proposed due to the existence of $Li(Na)BH_4$ [33,37]. Therefore, the $Li(Na)BH_4$ solid solution is formed in the as-milled LiNa-Ni mixture even though it is not observed in the PXD and Raman data. The corresponding phase transition temperatures during cooling of the LiNa-Ni and LiNa mixtures are both 89 ± 1 °C. This temperature is lower than that during heating as a consequence of under-cooling [33].

From DSC data the fusion and solidification onset temperatures of the as-milled LiNa-Ni mixture are determined to be 225 ± 1 °C and 222 ± 1 °C, respectively, influenced by a minor under-cooling effect. These temperatures are similar to those for the Ni-free sample (227 ± 1 °C and 222 ± 1 °C), suggesting the addition of 9 mol% of nano-sized Ni does not change the melting point for the $0.62LiBH_4$-$0.38NaBH_4$ mixture. However, by integration the area of those events, it is found that the phase transition areas are slightly reduced (Table B. 4 in Supporting Information). These areas are linearly proportional to the enthalpy.

3.3 Dehydrogenation Behavior

The TPD-MS trace for the dehydrogenation of the as-milled LiNa-Ni mixture is compared with the as-milled LiNa mixture in Figure 4.
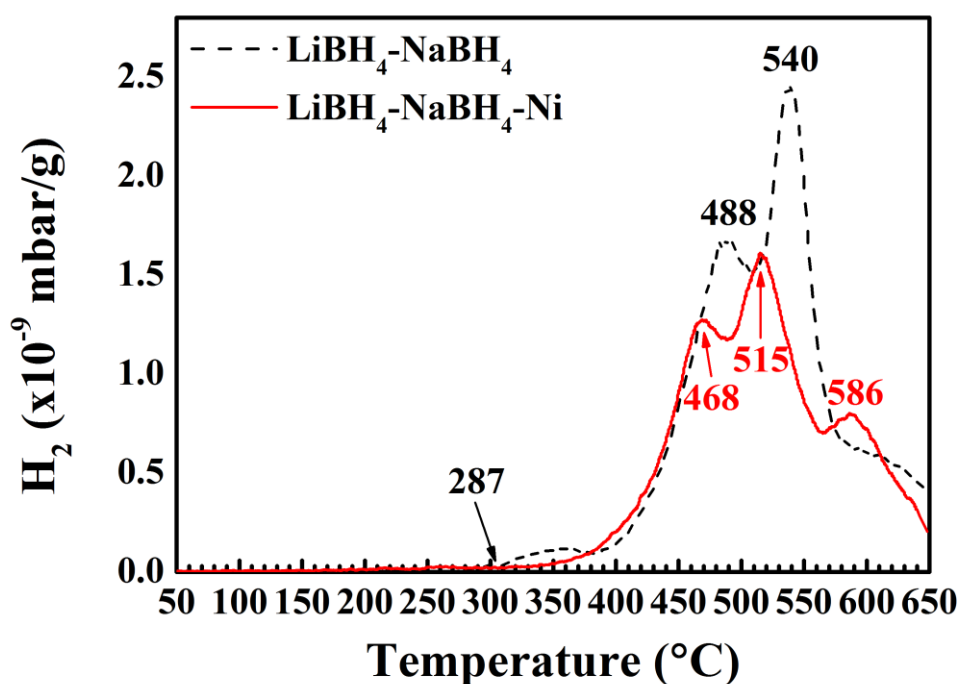
Figure 4 TPD-MS data show hydrogen desorption of the as-milled $0.91(0.62LiBH_4$-$0.38NaBH_4)$-$0.09Ni$ mixture (red solid curve), compared with that for the as-milled $0.62LiBH_4$-$0.38NaBH_4$ mixture (black dash curve). Samples were heated at 2 °C min^{-1} in flowing Ar at 160 mL min^{-1} between 50 and 650 °C.

The LiNa-Ni mixture starts to release H_2 from a relatively low temperature between 150-200 °C (Figure B. 2 in Supporting Information), which is about 50 °C lower than its melting point (225 °C) and about 100 °C lower than the dehydrogenation onset temperature (287 °C) for the Ni-free sample. However, a very limited amount of H_2 is released in this low temperature range.

The major dehydrogenation of the LiNa-Ni mixture starts above 350 °C, which is much lower than the 400 °C for the Ni-free sample. During decomposition, three peaks corresponding to three different dehydrogenation steps are observed at 468 °C, 515 °C and 586 °C. The peak temperatures for the 1st and 2nd peaks are 20 °C and 25 °C lower than the peaks at 488 °C and 540 °C for the Ni-free mixture. The 3rd peak at 586 °C is not observed in the Ni-free sample, suggesting a different decomposition pathway. Therefore, the dehydrogenation of LiNa-Ni mixture can be roughly divide into three ranges accordingly: 300-490 °C, 490-565 °C and 565-650 °C.

A total of 8.1 wt.% of hydrogen is released from LiNa-Ni upon heating to 650 °C in Ar. This value is calculated from the TPD-MS data (Figure 4) using the method described in Ref. [37]. When the weight of additives (17.8 wt%) is excluded, the $LiBH_4$-$NaBH_4$ content liberates 9.9 wt.% of hydrogen. The latter value is 9% less than the 10.9 wt.% for the Ni-free sample. B_2H_6 gas [75] is not detected during dehydrogenation of any sample in this work due to the experimental set-up whereby the mass spectrometer is connected to the TPD frame via a heated capillary tube and so the amount of gas that is able to reach the detector is limited. Therefore, the presence of a small amount of B_2H_6 cannot be ruled out.

3.4 Decomposition Pathways
Figure 5 summarizes the RT PXD results of as-milled LiNa-Ni mixture and LiNa-Ni samples heat-treated at 250 °C, 468 °C, 515 °C, 586 °C and 650 °C.
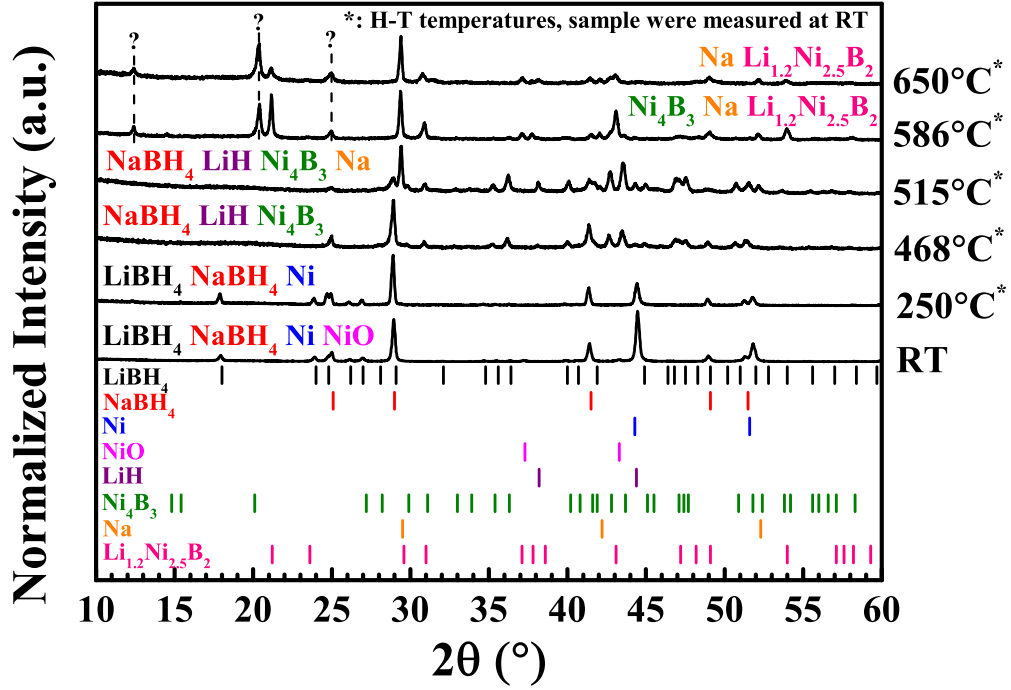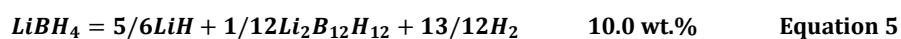
Figure 5 RT PXD pattern (Cu K$_\alpha$, λ = 1.5418 Å) of 0.91(0.62LiBH$_4$-0.38NaBH$_4$)-0.09Ni mixtures heat-treated at 250 °C, 468 °C, 515 °C, 586 °C and 650 °C in flowing Ar. Vertical ticks mark the Bragg peak positions for the found compounds. The intensities are normalized. Dashed lines were added as a guide for the eye.

In general, the PXD patterns in Figure 5 only indicate the stable phases at room temperature that provide guidance for a general understanding of the dehydrogenation. Due to the fact that LiH (T$_{melt}$ = 687.6 ± 0.8 °C), B (T$_{melt}$ = 2052.8 ± 21.3 °C) and Ni$_4$B$_3$ (T$_{melt}$ = 1007.55 °C) have higher melting points [76,77] than the heat-treatment temperatures (max. 650 °C) used in this work, their presences in the product remain solid once precipitated. Though the melting point of Li$_{1.2}$Ni$_{2.5}$B$_2$ has not been reported, Ref [78] suggested it is stable in crystalline structure to 760 °C. Thus, it is expected to be in its solid-state in the decomposition products. In addition, the metallic Na has a low melting point at 97.5 ± 0.6 °C [77], and thus stays in its liquid form once formed. However, unstable or intermediate phases are not represented but cannot be ruled out.

In order to investigate the solid-state reactions occurring in the low temperature range (150-250 °C), as-milled LiNa-Ni mixture was heated to 250 °C; this is

below the temperature where major dehydrogenation started in Ar. After heat-treatment, Bragg peaks of NiO disappear (Figure 5); indicating reactions between the parent borohydrides (very likely $LiBH_4$) and NiO. According to Ref. [79], $LiMO_x$ (M = transition metal) was observed as the main reaction product in a reaction involving transition metal oxide (MO_x) and $LiBH_4$. Thus, the formation of $Li_xNi_yO_z$ (i.e. Li_xNiO_2, x =0.25, 0.33, 04, 0.75, 1 [80]) is expected in our work. However, no Bragg peaks of a possible reaction product $Li_xNi_yO_z$ have been observed by PXD at RT. In addition, a separate study of $LiBH_4$-Ni (14 wt.% Ni) systems with bulk (3 μm) and nano-sized Ni ($\sim$ 100 nm) (Figure D. 1 in Supporting Information) indicates that the reduction of the dehydrogenation peak temperatures of LiNa-Ni (Figure 4) is caused by the addition of nano-sized Ni.

The PXD data for the sample heat-treated at 468 °C (Figure 5) show LiH, Ni_4B_3 and $NaBH_4$ phases. The formation of Ni_4B_3 is caused by the reaction between $LiBH_4$ and nano-sized Ni (Equation 1) leading to a 20 °C reduction of dehydrogenation peak temperature compared to the Ni-free sample, and thus in agreement with the literature [60]. However, other possible reaction products such as Ni_2B (Equation 2) or Ni_3B (Equation 3) [60] are not observed, suggesting these reactions have not occurred under the applied conditions or reaction products are amorphous. Signals related to $Li_2B_{10}H_{10}$ (i.e. most intensive Bragg peaks at 14.5, 15.7, 17.8 and 18.8 2θ°) [81] or $Li_2B_{12}H_{12}$ (i.e. most intensive Bragg peaks at 16.0 and 18.5 2θ°) [82] are not observed in the PXD patterns. However, the corresponding Raman spectra (Figure B. 3 in Supporting Information) present signals of remaining $NaBH_4$ (1276 cm^{-1}), B (1121 cm^{-1} and 1191 cm^{-1}), and $Li_2B_{12}H_{12}$ (765 cm^{-1}). The identification of LiH from PXD, as well as B and $Li_2B_{12}H_{12}$ from Raman spectroscopy confirm the decomposition of $LiBH_4$ via two competing decomposition pathways as suggested in Equation 4 and 5. There is no evidence of the decomposition of $NaBH_4$, which is in good agreement with the Ni-free sample [37]. Thus the 1st dehydrogenation step (300-490 °C) is associated with the reaction between $LiBH_4$ and nano-sized Ni along with the dehydrogenation of $LiBH_4$ in the mixture.

$$LiBH_4 = LiH + B + 3/2H_2 \qquad\qquad \text{13.9 wt.\%} \qquad \text{Equation 4}$$

$$LiBH_4 = 5/6LiH + 1/12Li_2B_{12}H_{12} + 13/12H_2 \qquad \text{10.0 wt.\%} \qquad \text{Equation 5}$$

At 515 °C, Bragg peaks of elemental Na, LiH and Ni_4B_3, along with weak peaks from $NaBH_4$, are observed in the PXD pattern (Figure 5). This indicates H_2 release mainly due to dehydrogenation of $NaBH_4$ for the 2nd dehydrogenation step (490-565 °C). The corresponding Raman spectra at this temperature (Figure B. 3 in Supporting Information) shows $[B_{12}H_{12}]^{2-}$ (762 cm^{-1}), B (1112 cm^{-1}), and two unknown peaks at 1249 cm^{-1} and 1224 cm^{-1} (shoulder).

At 586 °C, where the 3rd dehydrogenation step occurs, phases such as $Li_{1.2}Ni_{2.5}B_2$, Ni_4B_3 and Na are present in the PXD pattern (Figure 5), but the Bragg peaks of LiH have disappeared. $Li_{1.2}Ni_{2.5}B_2$ has not been observed in any other sample heat-treated at lower temperatures. Its existence is in agreement with the formation of $Li_{1.2}Ni_{2.5}B_2$ at 600 °C for $2LiBH_4$-Ni (micro-sized Ni ~ 41 μm) [83]. $Li_{1.2}Ni_{2.5}B_2$ is stable and it is observed in the PXD pattern of the sample heat-treated at 650 °C, where Ni_4B_3 has disappeared. The corresponding Raman spectra at 586 °C (Figure B. 3 in Supporting Information) shows $[B_{12}H_{12}]^{2-}$ (752 cm^{-1}), and three unknown peaks at 1059 cm^{-1}, 1173 cm^{-1} and 1220 cm^{-1}. The signals of B are not observed. Thus the dehydrogenation reaction occurring at this temperature is proposed to a chemical reaction between LiH, B and Ni_4B_3 that forms $Li_{1.2}Ni_{2.5}B_2$, H_2 and unknown phase(s).

Furthermore, it has been found that the position of the boron breathing mode (ν_2) of the $[B_{12}H_{12}]^{2-}$ red shifts with increasing heat-treatment temperature (Figure B. 3 in Supporting Information). This reduction in wavenumber is possibly due to the formation of $Na_2B_{12}H_{12}$ or a solid solution: $Li_xNa_{1-x}B_{12}H_{12}$, since the Raman shift of $Na_2B_{12}H_{12}$ was about 20 cm^{-1} lower than that of $Li_2B_{12}H_{12}$ [84] and the addition of Ni facilitated the formation of metal dodecaborates [85]. A degradation of the boron skeleton of $[B_{12}H_{12}]^{2-}$ could cause a shift of wavenumbers. However, this is unlikely to occur due to the stable cluster structure [86]. Moreover, lithium borates (such as LiB_3O_5, Li_2BO_2, $Li_2B_4O_7$,

$Li_4B_2O_5$) have been ruled out as contributing towards the unknown Raman peaks in the heat-treated samples at 515 and 586 °C [87–91].

3.5 Recombination

The measured (Meas.) H_2 release during cycling (Figure C. 1 in Supporting Information) for the LiNa and LiNa-Ni mixtures are summarized in Table 1. The corrected values (Corr.) exclude the weight of additive.

Table 1 Measured (Meas.) hydrogen release (wt.%) of 0.91(0.62LiBH₄-0.38NaBH₄)-0.09Ni during cycling (500 °C, 1 bar H₂ and 10 h for desorption, and 400 °C, 130 bar H₂ and 12 h for absorption), compared with 0.62LiBH₄-0.38NaBH₄. The corrected values (Corr.) are found by disregarding the weight of the Ni additive.

| H (wt.%)	LiBH₄-NaBH₄	LiBH₄-NaBH₄-Ni	
	Meas.	Meas.	Corr.
1st cycle	5.5	5.1 →	6.2
2nd cycle	1.1	1.1 →	1.3
3rd cycle	0.8	0.6 →	0.7

The LiNa mixture releases 5.5 wt.% of hydrogen during the 1st dehydrogenation (Table 1). The amount of hydrogen desorbed under the same conditions after reabsorption decreases dramatically to 1.1 wt.% at the 2nd cycle and further to 0.8 wt.% at the 3rd cycle. This poor cycling stability agrees with Ref. [28].

The LiNa-Ni mixture releases 6.2 wt.% of hydrogen (corrected value) during the 1st dehydrogenation (Table 1), which is 13 % higher than the 5.5 wt.% for the Ni-free sample, due to the destabilization effect of the nano-sized Ni additive. After rehydrogenation, the LiNa-Ni mixture absorbs 1.3 wt.% of hydrogen (corrected value) at the 2nd cycle, which is slightly higher than the 1.1 wt.% for the Ni-free sample. In addition, the reversible hydrogen content at the 3rd cycle for the LiNa-Ni mixture is 0.7 wt.% (corrected value), which is slight lower than the 0.8 wt.% for the Ni-free sample. Nevertheless, the reversible hydrogen contents of LiNa-Ni mixture at the 2nd and 3rd cycles are significantly reduced in contrast to that for the 1st cycle, which is not expected due to the Ni-induced high reabsorption

capacity of LiBH$_4$ [60]. This may be caused by the use of much harsher rehydrogenation conditions (350 bar, 550 °C, 24 h) in Ref. [60].

Figure 6 and Figure 7 show PXD and FTIR results for the LiNa and LiNa-Ni samples in their reabsorbed state after being cycled three times.
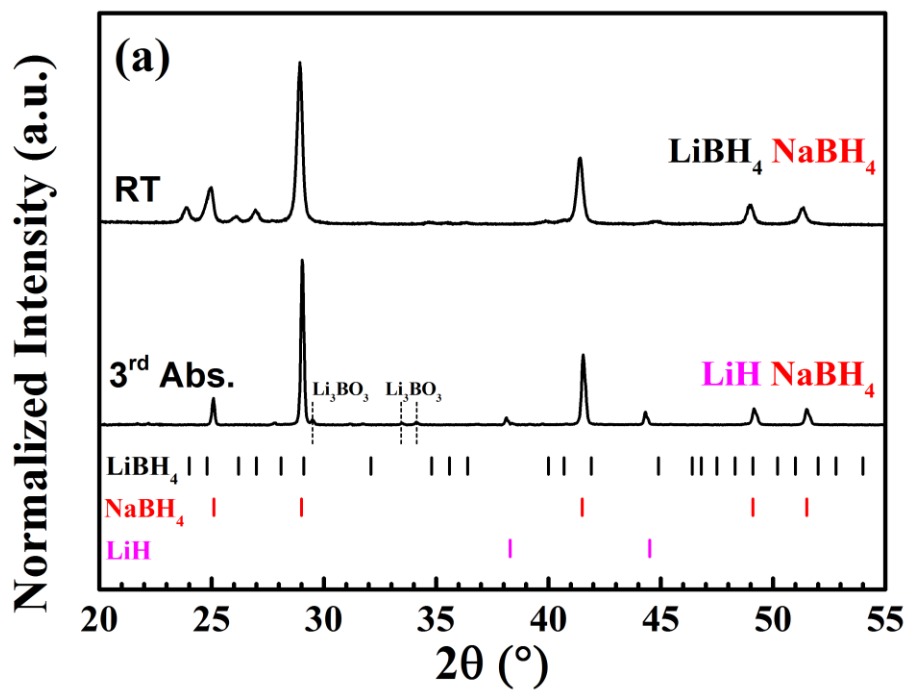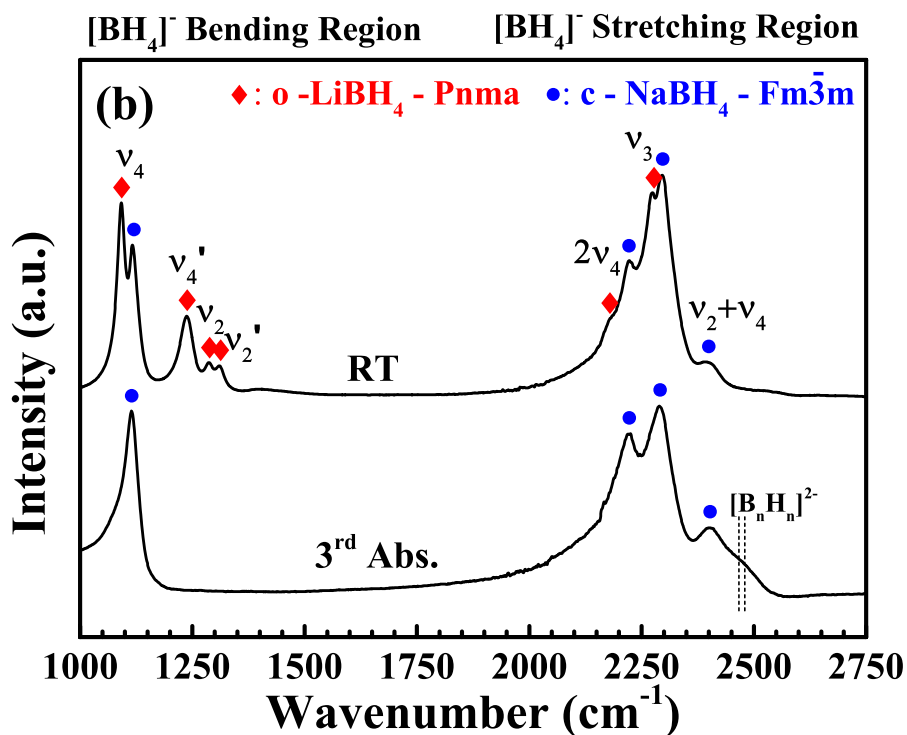
Figure 6 (a) PXD patterns (Cu K$_\alpha$, λ = 1.5418 Å) and (b) FTIR spectra of 0.62LiBH$_4$-0.38NaBH$_4$ decomposed at 500 °C in 1 bar static H$_2$ for 10 h and recombined in 130 bar H$_2$, 400 °C for 12 h at 3rd reabsorbed states (denoted as 3rd Abs.), compared with the as-milled sample (denoted as RT).
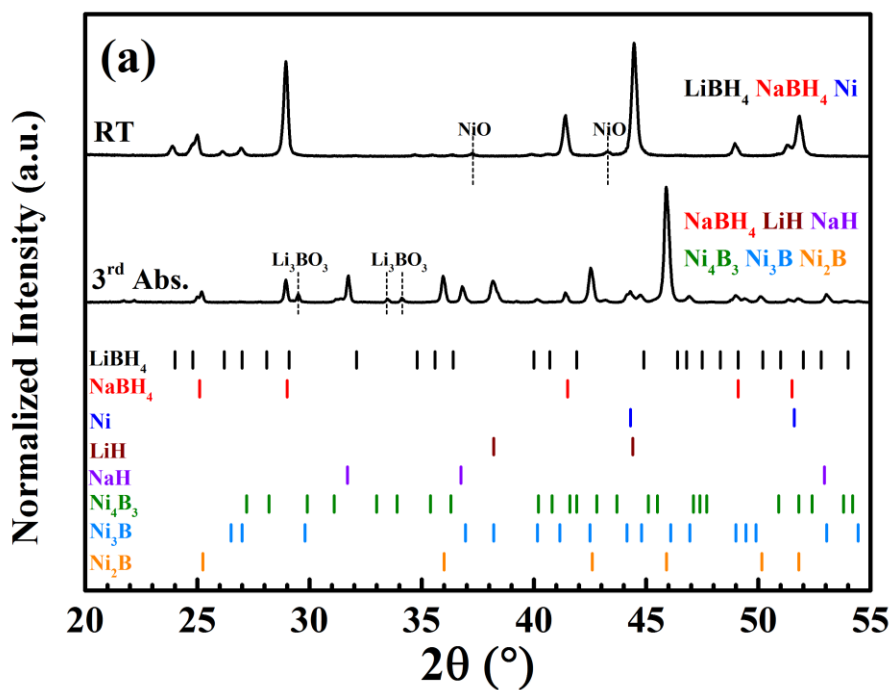
Figure 7 (a) PXD patterns (Cu Kα, λ = 1.5418 Å) and (b) FTIR spectra of 0.91(0.62LiBH₄-0.38NaBH₄)-0.09Ni decomposed at 500 °C in 1 bar static H₂ for 10 h and recombined in 130 bar H₂, 400 °C for 12 h at 3ʳᵈ reabsorbed states (denoted as 3ʳᵈ Abs.), compared with the as-milled sample (denoted as RT).
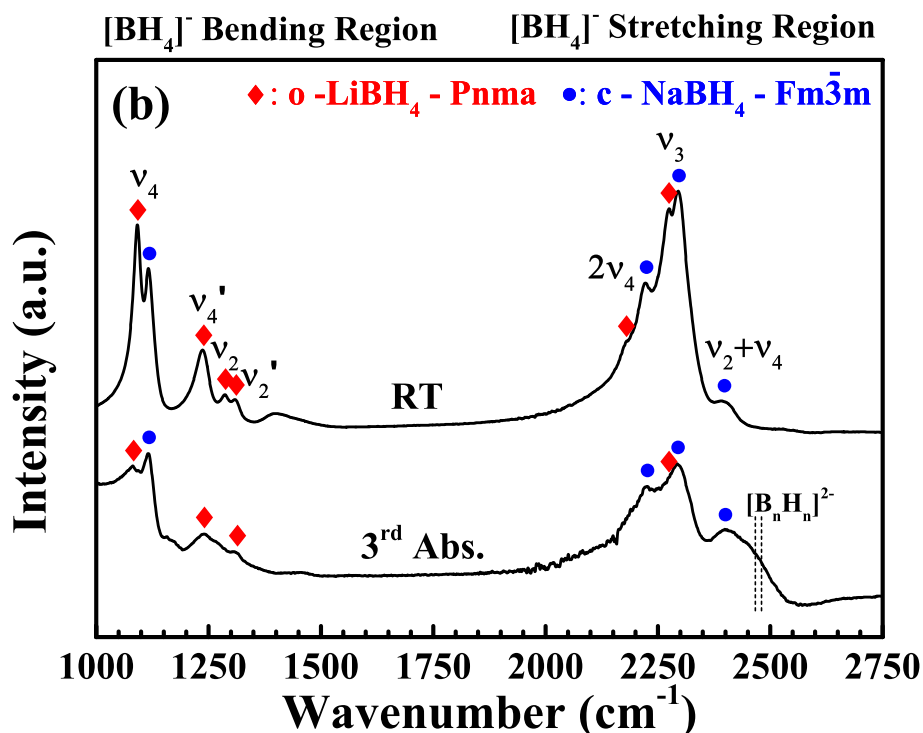
The three-time rehydrogenated LiNa mixture (Figure 6) contains LiH (PXD) and NaBH₄ (PXD, FTIR), indicating the NaBH₄ component is stable during cycling and the LiBH₄ component is not reversible under the applied conditions. The LiBH₄ is not fully decomposed after being kept at 500 °C in 1 bar H₂ for 10 h (Figure C. 2 in Supporting Information). Thus, the small amount of reabsorbed hydrogen contents at the 2ⁿᵈ and 3ʳᵈ cycle (Table 1) may be mainly due to the dehydrogenation of the remaining LiBH₄.

The PXD pattern of the three-time rehydrogenated LiNa-Ni mixture (Figure 7) shows Bragg peaks of NaBH₄, LiH, NaH, Ni₄B₃, Ni₃B and Ni₂B phases, indicating the occurrence of: reactions of LiBH₄ with Ni; decomposition of LiBH₄; and partial decomposition of NaBH₄ during the cycling. Due to the addition of nano-sized Ni, LiBH₄ is found to be fully decomposed after the first dehydrogenation process as no LiBH₄ signal has been observed in either PXD or FTIR result (Figure C. 3 in Supporting Information). A broad shoulder peak at around 2470

cm^{-1} is found in the FTIR data for the reaction product of LiNa-Ni at the 1st dehydrogenated state (Figure C. 3 in Supporting Information), which is due to the formation of closo-boranes ($[B_{10}H_{10}]^{2-}$ at ~2467 cm^{-1} or $[B_{12}H_{12}]^{2-}$ at ~2480 cm^{-1}) [92,93]. This broad peak has not been observed by FTIR for the dehydrogenation product of the Ni-free sample at the same state (Figure C. 2 in Supporting Information), confirming the addition of Ni facilitates the formation of dodecaborates, as mentioned in Ref. [85].

The Bragg peaks of NaH are first found in the PXD pattern for the dehydrogenation product of LiNa-Ni after being kept at 500 °C in 1 bar H$_2$ for 10 h (Figure C. 3 in Supporting Information) and its observation can be explained as follows: due to the low boiling point of Na (i.e. 281 °C at 10^{-5} bar of Na gas [94]), any reaction product Na (liquid) vaporizes immediately. The gaseous Na will condense when it reaches the colder part outside the hot zone (might further solidify, subject to temperature). The escaped Na reacts in an exothermic reaction with gaseous H$_2$ to form NaH, leading to a physical segregation of decomposition products [95]. The hydrogenation of Na was also noted to occur at 300 °C in 2-3 bar H$_2$ [96]. Thus, when the decomposition occurs in Ar, NaH is not observed (Figure 5). To prevent such eventualities, Na could be physically or chemically confined using nano-scaffolds (nanoconfinement) or metal fluorides [97] or closed containers [98].

In addition, Ni$_4$B$_3$ is one of the major dehydrogenation products of the LiNa-Ni mixture after being kept at 500 °C in 1 bar H$_2$ for 10 h (Figure C. 3 in Supporting Information). It could convert to Ni$_3$B after rehydrogenation, and Ni$_3$B could be further oxidized by B to Ni$_2$B [95]. Since the Bragg peaks for NaH disappear after the first rehydrogenation step (Figure C. 3 in Support Information), it is proposed that NaH reacts with Ni$_4$B$_3$ under H$_2$ and consequently forms NaBH$_4$ and Ni$_3$B during H$_2$ absorption.

After being cycled 3 times, the FTIR data (Figure 7) for the rehydrogenated LiNa-Ni mixture show peaks at 1079 cm^{-1}, 1238 cm^{-1}, 1308 cm^{-1} and a shoulder around 2270 cm^{-1}. These peaks are similar to LiBH$_4$ (i.e. 1091 cm^{-1}, 1236 cm^{-1},

1308 cm^{-1} and a 2273 cm^{-1} in as-milled LiNa-Ni), suggesting an amorphous LiBH$_4$ phase is reformed, which can be attributed to the catalytic effect of Ni$_4$B$_3$ on rehydrogenation [60].

Broad signals around 2400-2500 cm^{-1} have been noticed in the FTIR data for the rehydrogenated LiNa (Figure 6) and LiNa-Ni (Figure 7), indicating the formation of [B$_{10}$H$_{10}$]$^{2-}$ (~2467 cm^{-1}) [92] or [B$_{12}$H$_{12}$]$^{2-}$ (~2480 cm^{-1}) [93]. However, none of the mentioned dodecaboranes could be identified from the corresponding PXD data, where we would have expected Bragg peaks in the low 2θ range (15-20 2θ°) [81,82], thus indicating that they could be present in an amorphous or nano-crystalline state.

Although the cycling stability of the LiNa mixture has not been significantly improved by adding nano-sized Ni particles, the reaction product Ni$_4$B$_3$ facilitates the reformation of LiBH$_4$ under much milder conditions (lower temperature and pressure) than reported before [60].

4 Conclusions

The dehydrogenation mechanism of the 0.91(0.62LiBH$_4$-0.38NaBH$_4$)-0.09Ni mixture is systematically studied between 25 °C and 650 °C in flowing Ar. The addition of 9 mol% nano-sized Ni powder does not affect the low orthorhombic to hexagonal LiBH$_4$ phase transition temperature (99 °C) and the low melting temperature (225 °C), whilst it reduces the dehydrogenation peak temperatures by 20-25 °C, leading to three major decomposition steps, from:

1) 300 °C to 490 °C, H$_2$ release is associated with a reaction between LiBH$_4$ and nano-sized Ni (forming LiH and Ni$_4$B$_3$), along with the dehydrogenation of the LiBH$_4$ component in the mixture, forming LiH, B, Li$_2$B$_{12}$H$_{12}$;

2) 490 °C to 565 °C, the dehydrogenation is mainly due to the decomposition of the NaBH$_4$ component, forming Na, B, and possibly Na$_2$B$_{12}$H$_{12}$;

3) 565 °C to 650 °C, H$_2$ liberation is due to a reaction between LiH, B and Ni$_4$B$_3$, forming Li$_{1.2}$Ni$_{2.5}$B$_2$ and unknown phases.

A total of 8.1 wt.% of hydrogen is released upon heating to 650 °C in Ar, which is lower than 10.9 wt.% of the Ni-free mixture. This $0.91(0.62LiBH_4\text{-}0.38NaBH_4)\text{-}0.09Ni$ mixture has a poor cycling stability as its reversible hydrogen content reduced from 5.1 wt.% to 1.1 wt.% to 0.6 wt.% during three complete desorption-absorption-cycles. However, it is suggested that its $LiBH_4$ content is partially reversible under much milder conditions than reported before [60].

5 Acknowledgements

6 References

[1]   Rusman NAA, Dahari M. A review on the current progress of metal hydrides material for solid-state hydrogen storage applications. Int J Hydrogen Energy 2016;41:12108–26. doi:10.1016/j.ijhydene.2016.05.244.

[2]   Liu C, Li F, Ma LP, Cheng HM. Advanced Materials for Energy Storage. Adv Mater 2010;22:E28–62. doi:DOI 10.1002/adma.200903328.

[3]   David WIF. Effective hydrogen storage: a strategic chemistry challenge. Faraday Discuss 2011;151:399–414. doi:10.1039/c1fd00105a.

[4]   Jain IP, Jain P, Jain A. Novel hydrogen storage materials: A review of lightweight complex hydridespuye. J Alloys Compd 2010;503:303–39. doi:10.1016/j.jallcom.2010.04.250.

[5]   Li HW, Yan Y, Orimo SI, Züttel A, Jensen CM. Recent progress in metal borohydrides for hydrogen storage. Energies 2011;4:185–214. doi:10.3390/en4010185.

[6]   Mohtadi R, Remhof A, Jena P. Complex metal borohydrides: multifunctional materials for energy storage and conversion. J Phys Condens Matter 2016;28:353001. doi:10.1088/0953-8984/28/35/353001.

[7]   Ren J, Musyoka NM, Langmi HW, Mathe M, Liao S. Current research trends and perspectives on materials-based hydrogen storage solutions: A critical review. Int J Hydrogen Energy 2017;42:289–311. doi:10.1016/j.ijhydene.2016.11.195.

[8]   Züttel A, Wenger P, Rentsch S, Sudan P, Mauron P, Emmenegger C, et al. LiBH4 a new hydrogen storage material. J Power Sources 2003;118:1–7. doi:10.1016/S0378-7753(03)00054-5.

[9]   Züttel A, Rentsch S, Fischer P, Wenger P, Sudan P, Mauron P, et al. Hydrogen storage properties of LiBH4. J Alloys Compd 2003;356–357:515–20. doi:10.1016/S0925-8388(02)01253-7.

[10] Mohtadi R, Orimo S. The renaissance of hydrides as energy materials. Nat Rev Mater 2016;2:16091. doi:10.1038/natrevmats.2016.91.

[11] Paskevicius M, Jepsen LH, Schouwink P, Černý R, Ravnsbæk DB, Filinchuk Y, et al. Metal borohydrides and derivatives – synthesis, structure and properties. Chem Soc Rev 2017;46:1565–634. doi:10.1039/C6CS00705H.

[12] Callini E, Atakli ZÖK, Hauback BC, Orimo S, Jensen C, Dornheim M, et al. Complex and liquid hydrides for energy storage. Appl Phys A 2016;122:353. doi:10.1007/s00339-016-9881-5.

[13] Zavorotynska O, El-Kharbachi A, Deledda S, Hauback BC. Recent progress in magnesium borohydride Mg(BH4)2: Fundamentals and applications for energy storage. Int J Hydrogen Energy 2016;41:14387–403. doi:10.1016/j.ijhydene.2016.02.015.

[14] Orimo S-I, Nakamori Y, Eliseo JR, Züttel A, Jensen CM. Complex hydrides for hydrogen storage. Chem Rev 2007;107:4111–32. doi:10.1021/cr0501846.

[15] Zuttel A, Remhof A, Borgschulte A, Friedrichs O. Hydrogen: the future energy carrier. Philos Trans R Soc A Math Phys Eng Sci 2010;368:3329–42. doi:10.1098/rsta.2010.0113.

[16] Lee JY, Ravnsbæk D, Lee Y-S, Kim Y, Cerenius Y, Shim J-H, et al. Decomposition Reactions and Reversibility of the LiBH4–Ca(BH4)2 Composite. J Phys Chem C 2009;113:15080–6. doi:10.1021/jp904400b.

[17] Paskevicius M, Ley MB, Sheppard DA, Jensen TR, Buckley CE. Eutectic melting in metal borohydrides. Phys Chem Chem Phys 2013;15:19774–89. doi:10.1039/c3cp53920b.

[18] Yan Y, Remhof A, Mauron P, Rentsch D, Lodziana Z, Lee Y-S, et al. Controlling the Dehydrogenation Reaction toward Reversibility of the LiBH4–Ca(BH4)2 Eutectic System. J Phys Chem C 2013;117:8878–86. doi:10.1021/jp401628g.

[19] Nale A, Catti M, Bardají EG, Fichtner M. On the decomposition of the 0.6LiBH4-0.4Mg(BH4)2 eutectic mixture for hydrogen storage. Int J Hydrogen Energy 2011;36:13676–82. doi:10.1016/j.ijhydene.2011.08.009.

[20] Bardají EG, Zhao-Karger Z, Boucharat N, Nale A, van Setten MJ, Lohstroh W, et al. LiBH4–Mg(BH4)2 : A Physical Mixture of Metal Borohydrides as Hydrogen Storage Material. J Phys Chem C 2011;115:6095–101. doi:10.1021/jp110518s.

[21] Chen J, Zhang Y, Xiong Z, Wu G, Chu H, He T, et al. Enhanced hydrogen desorption from the Co-catalyzed LiBH4–Mg(BH4)2 eutectic composite. Int J Hydrogen Energy 2012;37:12425–31. doi:10.1016/j.ijhydene.2012.06.057.

[22] Ley MB, Roedern E, Jensen TR. Eutectic melting of LiBH4-KBH4. Phys Chem Chem Phys 2014;16:24194–9. doi:10.1039/c4cp03207a.

[23] Xu X, Zang L, Zhao Y, Zhao Y, Wang Y, Jiao L. Hydrogen storage behavior of LiBH4 improved by the confinement of hierarchical porous ZnO/ZnCo2O4 nanoparticles. J Power Sources 2017;359:134–41. doi:10.1016/j.jpowsour.2017.05.047.

[24] Yan Y, Remhof A, Rentsch D, Züttel A. The role of MgB12H12 in the hydrogen desorption process of Mg(BH4)2. Chem Commun 2015;51:700–2. doi:10.1039/C4CC05266H.

[25]   Yan Y, Rentsch D, Battaglia C, Remhof A. Synthesis, stability and Li-ion mobility of nanoconfined Li2B12H12. Dalt Trans 2017;46:12434–7. doi:10.1039/C7DT02946B.

[26]   Lee HS, Lee YS, Suh JY, Kim M, Yu JS, Cho YW. Enhanced desorption and absorption properties of eutectic LiBH4-Ca(BH4)2 infiltrated into mesoporous carbon. J Phys Chem C 2011;115:20027–35. doi:10.1021/jp206000h.

[27]   Zhao-Karger Z, Witter R, Bardají EG, Wang D, Cossement D, Fichtner M. Altered reaction pathways of eutectic LiBH4-Mg(BH4)2 by nanoconfinement. J Mater Chem A 2013;1:3379. doi:10.1039/c2ta00542e.

[28]   Javadian P, Sheppard DA, Buckley CE, Jensen TR. Hydrogen storage properties of nanoconfined LiBH4-NaBH4. Int J Hydrogen Energy 2015;40:14916–24. doi:10.1016/j.ijhydene.2015.08.075.

[29]   Javadian P, Jensen TR. Enhanced hydrogen reversibility of nanoconfined LiBH4–Mg(BH4)2. Int J Hydrogen Energy 2014;39:9871–6. doi:10.1016/j.ijhydene.2014.03.007.

[30]   Zhai B, Xiao X, Lin W, Huang X, Fan X, Li S, et al. Enhanced hydrogen desorption properties of LiBH4-Ca(BH4)2 by a synergetic effect of nanoconfinement and catalysis. Int J Hydrogen Energy 2016;41:17462–70. doi:10.1016/j.ijhydene.2016.06.170.

[31]   Roedern E, Hansen BRS, Ley MB, Jensen TR. Effect of Eutectic Melting, Reactive Hydride Composites, and Nanoconfinement on Decomposition and Reversibility of LiBH4-KBH4. J Phys Chem C 2015;119:25818–25. doi:10.1021/acs.jpcc.5b09228.

[32]   Jensen SRH, Jepsen LH, Skibsted J, Jensen TR. Phase Diagram for the NaBH4–KBH4 System and the Stability of a Na1– xKxBH4 Solid Solution. J Phys Chem C 2015;119:27919–29. doi:10.1021/acs.jpcc.5b09851.

[33]   Dematteis EM, Roedern E, Pinatel ER, Corno M, Jensen TR, Baricco M. A thermodynamic investigation of the LiBH4-NaBH4 system. RSC Adv 2016;6:60101–8. doi:10.1039/C6RA09301A.

[34]   Orimo S, Nakamori Y, Kitahara G, Miwa K, Ohba N, Towata S, et al. Dehydriding and rehydriding reactions of. J Alloys Compd 2005;404–406:427–30. doi:10.1016/j.jallcom.2004.10.091.

[35]   Urgnani J, Torres FJ, Palumbo M, Baricco M. Hydrogen release from solid state NaBH4. Int J Hydrogen Energy 2008;33:3111–5. doi:10.1016/j.ijhydene.2008.03.031.

[36]   Milanese C, Garroni S, Girella A, Mulas G, Berbenni V, Bruni G, et al. Thermodynamic and kinetic investigations on pure and doped NaBH4-MgH2 system. J Phys Chem C 2011;115:3151–62. doi:10.1021/jp109392e.

[37]   Liu Y, Reed D, Paterakis C, Contreras Vasquez L, Baricco M, Book D. Study of the decomposition of a 0.62LiBH 4 –0.38NaBH 4 mixture. Int J Hydrogen Energy 2017;42:22480–8. doi:10.1016/j.ijhydene.2017.03.141.

[38]   Yan Y, Remhof A, Hwang S-J, Li H-W, Mauron P, Orimo S, et al. Pressure and temperature dependence of the decomposition pathway of LiBH4. Phys Chem Chem Phys 2012;14:6514–9. doi:10.1039/c2cp40131b.

[39]   El Kharbachi A, Pinatel E, Nuta I, Baricco M. A thermodynamic assessment of LiBH4. Calphad Comput Coupling Phase Diagrams Thermochem 2012;39:80–90. doi:10.1016/j.calphad.2012.08.005.

[40]   Hwang SJ, Bowman RC, Reiter JW, Rijssenbeek J, Soloveichik GL, Zhao JC, et

al. NMR confirmation for formation of [B12H12]2- complexes during hydrogen desorption from metal borohydrides. J Phys Chem C 2008;112:3164–9. doi:10.1021/jp710894t.

[41] Huang Z-Q, Chen W-C, Chuang F-C, Majzoub EH, Ozoliņš V. First-principles calculated decomposition pathways for LiBH4 nanoclusters. Sci Rep 2016;6:26056. doi:10.1038/srep26056.

[42] Renewable O of EE&. HYDROGEN STORAGE n.d. http://energy.gov/eere/fuelcells/hydrogen-storage (accessed October 10, 2016).

[43] Siegel DJ, Wolverton C, Ozoliņš V. Thermodynamic guidelines for the prediction of hydrogen storage reactions and their application to destabilized hydride mixtures. Phys Rev B - Condens Matter Mater Phys 2007;76:1–6. doi:10.1103/PhysRevB.76.134102.

[44] Heere M, Payandeh GharibDoust SH, Frommen C, Humphries TD, Ley MB, Sørby MH, et al. The influence of LiH on the rehydrogenation behavior of halide free rare earth (RE) borohydrides (RE = Pr, Er). Phys Chem Chem Phys 2016;18:24387–95. doi:10.1039/C6CP04523E.

[45] Heere M, GharibDoust S, Brighi M, Frommen C, Sørby M, Černý R, et al. Hydrogen Sorption in Erbium Borohydride Composite Mixtures with LiBH4 and/or LiH. Inorganics 2017;5:31. doi:10.3390/inorganics5020031.

[46] Au M, Jurgensen AR, Spencer WA, Anton DL, Pinkerton FE, Hwang SJ, et al. Stability and reversibility of lithium borohydrides doped by metal halides and hydrides. J Phys Chem C 2008;112:18661–71. doi:10.1021/jp8024304.

[47] Zhang BJ, Liu BH. Hydrogen desorption from LiBH4 destabilized by chlorides of transition metal Fe, Co, and Ni. Int J Hydrogen Energy 2010;35:7288–94. doi:10.1016/j.ijhydene.2010.04.165.

[48] Vajo JJ, Skeith SL, Mertens F. Reversible storage of hydrogen in destabilized LiBH 4. J Phys Chem B 2005;109:3719–22. doi:10.1021/jp040769o.

[49] Pinkerton FE, Meyer MS. Reversible hydrogen storage in the lithium borohydride-calcium hydride coupled system. J Alloys Compd 2008;464:4–7. doi:10.1016/j.jallcom.2007.09.125.

[50] Ibikunle A, Goudy AJ, Yang H. Hydrogen storage in a CaH2/LiBH4 destabilized metal hydride system. J Alloys Compd 2009;475:110–5. doi:10.1016/j.jallcom.2008.08.010.

[51] Mao JF, Guo ZP, Liu HK, Yu XB. Reversible hydrogen storage in titanium-catalyzed LiAlH4-LiBH4 system. J Alloys Compd 2009;487:434–8. doi:10.1016/j.jallcom.2009.07.158.

[52] Shim JH, Lim JH, Rather S ullah, Lee YS, Reed D, Kim Y, et al. Effect of hydrogen back pressure on dehydrogenation behavior of LiBH4-based reactive hydride composites. J Phys Chem Lett 2010;1:59–63. doi:10.1021/jz900012n.

[53] Javadian P, Zlotea C, Ghimbeu CM, Latroche M, Jensen TR. Hydrogen storage properties of nanoconfined LiBH4-Mg2NiH4 reactive hydride composites. J Phys Chem C 2015;119:5819–26. doi:10.1021/jp5117307.

[54] Heere M, Sørby MH, Pistidda C, Dornheim M, Hauback BC. Milling time effect of Reactive Hydride Composites of NaF-NaH-MgB2 investigated by in situ powder diffraction. Int J Hydrogen Energy 2016;41:13101–8.

doi:10.1016/j.ijhydene.2016.05.153.

[55] Yuan PP, Liu BH, Li ZP. A comparative study of LiBH4-based composites with metal hydrides and fluorides for hydrogen storage. Int J Hydrogen Energy 2011;36:15266–72. doi:10.1016/j.ijhydene.2011.09.001.

[56] Gross AF, Vajo JJ, Van Atta SL, Olson GL. Enhanced Hydrogen Storage Kinetics of LiBH4 in Nanoporous Carbon Scaffolds. J Phys Chem C 2008;112:5651–7. doi:10.1021/jp711066t.

[57] Cahen S, Eymery JB, Janot R, Tarascon JM. Improvement of the LiBH4 hydrogen desorption by inclusion into mesoporous carbons. J Power Sources 2009;189:902–8. doi:10.1016/j.jpowsour.2009.01.002.

[58] Ngene P, Adelhelm P, Beale AM, Jong KP De, Jongh PE De. LiBH4 / SBA-15 Nanocomposites Prepared by Melt Infiltration under Hydrogen Pressure : Synthesis and Hydrogen Sorption Properties. J Phys Chem C 2010;114:6163–8. doi:10.1021/jp9065949.

[59] Liu X, Peaslee D, Jost CZ, Majzoub EH. Controlling the decomposition pathway of LiBH4 via confinement in highly ordered nanoporous carbon. J Phys Chem C 2010;114:14036–41. doi:10.1021/jp1055045.

[60] Li H, Yan Y, Akiba E, Orimo S. Improved Dehydrogenation and Rehydrogenation Properties of LiBH4 by Nanosized Ni Addition. Mater Trans 2014;55:1134–7. doi:10.2320/matertrans.MG201407.

[61] Saldan I, Hino S, Humphries TD, Zavorotynska O, Chong M, Jensen CM, et al. Structural Changes Observed during the Reversible Hydrogenation of Mg(BH4)2 with Ni-Based Additives. J Phys Chem C 2014;118:23376–84. doi:10.1021/jp5066677.

[62] Brown CA, Brown HC. The Reaction of Sodium Borohydride with Nickel Acetate in Aqueous Solution--A Convenient Synthesis of an Active Nickel Hydrogenation Catalyst of Low Isomerizing Tendency. J Am Chem Soc 1963;85:1003–5. doi:10.1021/ja00890a040.

[63] Bruker. EVA Software - The next era in phase analysis 2016.

[64] Coelho A. TOPAS Academic Version 4.1 2007.

[65] FIZ Karlsruhe. Inorganic Crystal Structure Databas (ICSD). 2017 n.d. http://icsd.cds.rsc.org/ (accessed February 16, 2017).

[66] Renishaw. WiRE 4 Software for Raman Spectroscopy from Renishaw n.d. http://www.renishaw.com/en/raman-software--9450 (accessed November 1, 2017).

[67] Brinks HW, Fossdal A, Bowman RC, Hauback BC. Pressure–composition isotherms of TbNiAlHx. J Alloys Compd 2006;417:92–5. doi:10.1016/j.jallcom.2005.09.018.

[68] Paterakis C, Guo S, Heere M, Liu Y, Contreras LF, Sørby MH, et al. Study of the NaBH4 –NaBr system and the behaviour of its low temperature phase transition. Int J Hydrogen Energy 2017;42:22538–43. doi:10.1016/j.ijhydene.2017.03.045.

[69] Gomes S, Hagemann H, Yvon K. Lithium boro-hydride LiBH4. J Alloys Compd 2002;346:206–10. doi:10.1016/S0925-8388(02)00668-0.

[70] Harvey KB, McQuaker NR. Infrared and Raman Spectra of Potassium and Sodium Borohydride. Can J Chem 1971;49:3272–81. doi:10.1139/v71-545.

[71] Reed D, Book D. Recent applications of raman spectroscopy to the study of complex hydrides for hydrogen storage. Curr Opin Solid State Mater Sci 2011;15:62–72. doi:10.1016/j.cossms.2010.12.001.

[72] Reed D, Book D. In-situ Raman study of the thermal decomposition of LiBH4. MRS Proc 2009;1216. doi:10.1557/PROC-1216-W06-05.

[73] Badger RM. A Relation Between Internuclear Distances and Bond Force Constants. J Chem Phys 1934;2:128–31. doi:10.1063/1.1749433.

[74] Renaudin G, Gomes S, Hagemann H, Keller L, Yvon K. Structural and spectroscopic studies on the alkali borohydrides MBH4 (M = Na, K, Rb, Cs). J Alloys Compd 2004;375:98–106. doi:10.1016/j.jallcom.2003.11.018.

[75] Friedrichs O, Remhof A, Hwang SJ, Züttel A. Role of Li2B12H12 for the formation and decomposition of LiBH4. Chem Mater 2010;22:3265–8. doi:10.1021/cm100536a.

[76] Franke P, Neuschütz D. B-Ni. Bin. Syst. Part 2 Elem. Bin. Syst. from B – C to Cr – Zr, Berlin/Heidelberg: Springer-Verlag; n.d., p. 1–4. doi:10.1007/10757405_11.

[77] Westhaus U. DETHERM. Gesellschaft Für Chem Tech Und Biotechnol eV n.d. http://dechema.de/en/detherm.html (accessed April 11, 2018).

[78] Jung W. Darstellung und Kristallstruktur von MgNi2.5B2 und Li1.2Ni2.5B2. Zeitschrift Fuer Naturforschung, Tl B Anorg Chemie, Org Chemie 1977:1371–4.

[79] Yu XB, Grant DM, Walker GS. Dehydrogenation of LiBH 4 Destabilized with Various Oxides 2009:17945–9.

[80] Arroyo y de Dompablo ME, Ceder G. First-principles calculations on LixNiO2: phase stability and monoclinic distortion. J Power Sources 2003;119–121:654–7. doi:10.1016/S0378-7753(03)00199-X.

[81] Wu H, Tang WS, Stavila V, Zhou W, Rush JJ, Udovic TJ. Structural behavior of Li2B10H10. J Phys Chem C 2015;119:6481–7. doi:10.1021/acs.jpcc.5b00533.

[82] Her J-H, Yousufuddin M, Zhou W, Jalisatgi SS, Kulleck JG, Zan JA, et al. Crystal Structure of Li2B12H12 : a Possible Intermediate Species in the Decomposition of LiBH4. Inorg Chem 2008;47:9757–9. doi:10.1021/ic801345h.

[83] Xia GL, Guo YH, Wu Z, Yu XB. Enhanced hydrogen storage performance of LiBH4–Ni composite. J Alloys Compd 2009;479:545–8. doi:10.1016/j.jallcom.2008.12.128.

[84] He L, Li H-W, Nakajima H, Tumanov N, Filinchuk Y, Hwang S-J, et al. Synthesis of a Bimetallic Dodecaborate LiNaB12H12 with Outstanding Superionic Conductivity. Chem Mater 2015;27:5483–6. doi:10.1021/acs.chemmater.5b01568.

[85] Ngene P, van Zwienen MR, de Jongh PE. Reversibility of the hydrogen desorption from LiBH4: a synergetic effect of nanoconfinement and Ni addition. Chem Commun (Camb) 2010;46:8201–3. doi:10.1039/c0cc03218b.

[86] Sivaev IB. Chemistry of closo- Dodecaborate Anion [B12H12]2- : A Review 2017. doi:10.1135/cccc20020679.

[87] Kowada Y, Tatsumisago M, Minami T. Raman spectra of rapidly quenched glasses in the systems lithium borate-lithium silicate-lithium phosphate (Li3BO3-Li4SiO4-Li3PO4 and Li4B2O5-Li6Si2O7-Li4P2O7). J Phys Chem 1989;93:2147–51. doi:10.1021/j100342a085.

[88] Xiong G, Lan G, Wang H, Huang C. Infrared reflectance and Raman spectra of lithium triborate single crystal. J Raman Spectrosc 1993;24:785–9.

doi:10.1002/jrs.1250241111.

[89] Jiang Y, Wang Y, Zeng L. Analysis of Raman Spectra of LiB3O5 Single Crystals. J Raman Spectrosc 1996;27:601–7. doi:10.1002/(SICI)1097-4555(199608)27:8<601::AID-JRS993>3.0.CO;2-P.

[90] Voronko YK, Sobol AA, Shukshin VE. Raman spectroscopy study of the phase transformations of LiB3O5 and Li2B4O7 during heating and melting. Inorg Mater 2013;49:923–9. doi:10.1134/S0020168513090203.

[91] Moiseenko VN, Vdovin A V., Dergachov MP. Raman scattering in lithium borate crystals. In: Gorelik VS, Kudryavtseva AD, editors., 2000, p. 36. doi:10.1117/12.378133.

[92] Leites LA. Vibrational Spectroscopy of Carboranes and Parent Boranes and Its Capabilities in Carborane Chemistry. Chem Rev 1992;92:279–323. doi:10.1021/cr00010a006.

[93] Muetterties EL, Merrifield RE, Miller HC, Knoth WH, Downing JR. Chemistry of Boranes. III. The Infrared and Raman Spectra of B12H12- and Related Anions. J Am Chem Soc 1962;84:2506–8. doi:10.1021/ja00872a011.

[94] GTT Technologies. SGTE Subst. database V 4.1 n.d. http://www.gtt-technologies.de/data/sgte-databases.

[95] Humphries TD, Kalantzopoulos GN, Llamas-Jansa I, Olsen JE, Hauback BC. Reversible Hydrogenation Studies of NaBH4 Milled with Ni-Containing Additives. J Phys Chem C 2013;117:6060–5. doi:10.1021/jp312105w.

[96] Dymova TN, Vysheslavtsev AA. Preparation of sodium hydride. Zhurnal Neorg Khimii 1960;5:2153–6.

[97] Mao J, Gregory D. Recent Advances in the Use of Sodium Borohydride as a Solid State Hydrogen Store. Energies 2015;8:430–53. doi:10.3390/en8010430.

[98] Sheppard DA, Humphries TD, Buckley CE. Sodium-based hydrides for thermal energy applications. Appl Phys A Mater Sci Process 2016;122:1–13. doi:10.1007/s00339-016-9830-3.

Supporting Information

Appendix A Analysis of as-received nano-sized Ni powder

Figure A. 1 shows the PXD pattern of the as-received nano-sized Ni at room temperature. Bragg peaks are mainly observed for the cubic Ni phase. Some low-intensity peaks associated with NiO are detected. The amount of NiO is 6.4 ± 0.2 wt.% according to QPA refinement results.
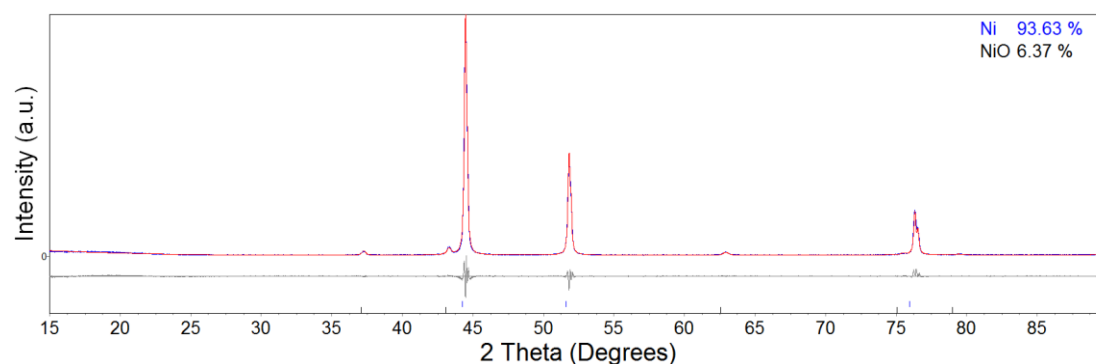

Figure A. 1 QPA refinement result of as-received nano-sized Ni, including the observed XRD (Cu K$_\alpha$, λ = 1.5418 Å) profile (blue), the calculated profile (red, used to fit the observed profile) and the difference profile (grey). Goodness-of-fit = 1.483.

The Philips XL-30 (LaB6) with Link Isis EDS Scanning Electron Microscope (SEM) was used to identify the size and morphology of nano-sized Ni powder (Figure A. 2). Powder agglomeration was observed.
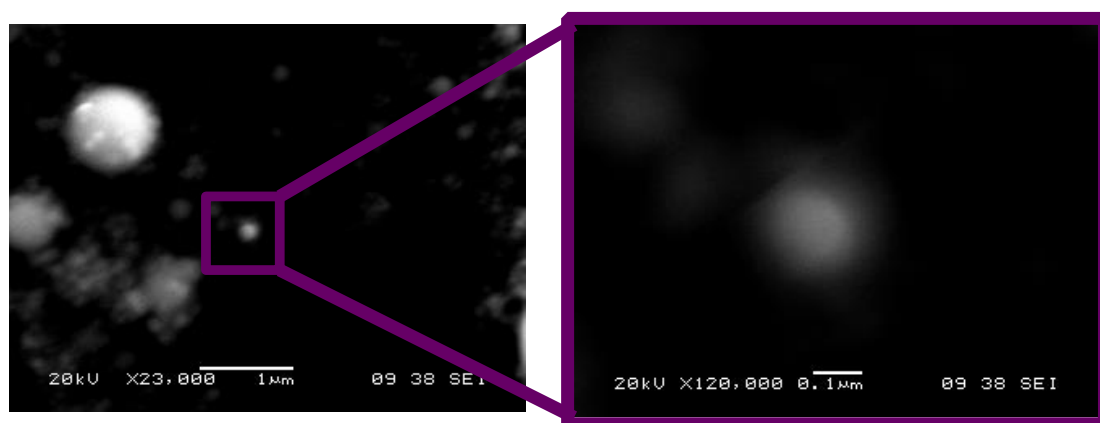

Figure A. 2 Secondary SEM images of as-received nano-sized Ni powder at room temperature.

Appendix B Analysis of LiBH$_4$-NaBH$_4$-Ni mixture

Figure B. 1 and Table B. 1 illustrate the TOPAS QPA refinement results of the as-milled 0.91(0.62LiBH$_4$-0.38NaBH$_4$)-0.09Ni mixture.
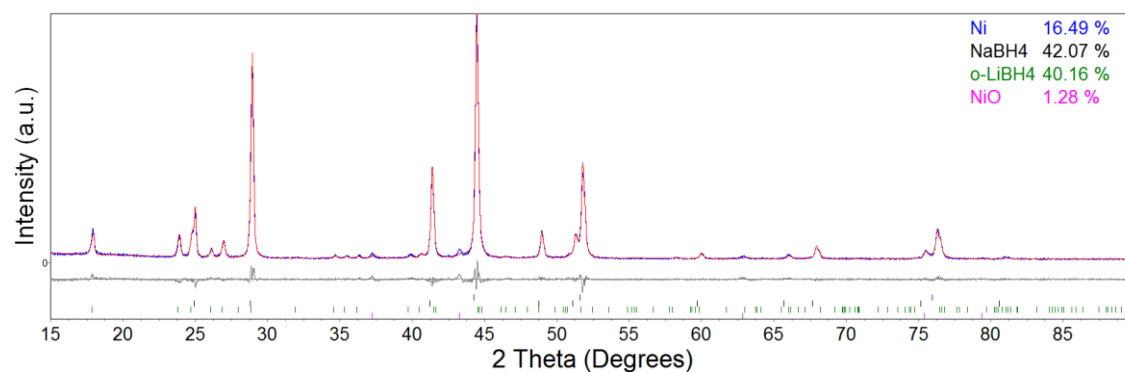
Figure B. 1 QPA refinement result of the as-milled 0.91(0.62LiBH$_4$-0.38NaBH$_4$)-0.09Ni mixture, including the observed XRD (Cu K$_\alpha$, λ = 1.5418 Å) profile (blue), the calculated profile (red, used to fit the observed profile) and the difference profile (grey). Goodness-of-fit = 1.459.

Table B. 1 Refined crystal structure parameters of the LiBH$_4$ and NaBH$_4$ components in the as-milled 0.91(0.62LiBH$_4$-0.38NaBH$_4$)-0.09Ni mixture in contrast to of as-milled 0.62LiBH$_4$-0.38NaBH$_4$ mixture

		As-milled Pure		As-milled Mixture	
		LiBH$_4$	NaBH$_4$	LiBH$_4$-NaBH$_4$	LiBH$_4$-NaBH$_4$-Ni
o-LiBH$_4$	a (Å)	7.199 ± 0.003	-	7.179 ± 0.002	7.211 ± 0.001
	b (Å)	4.438 ± 0.002	-	4.438 ± 0.001	4.456 ± 0.001
	c (Å)	6.798 ± 0.002	-	6.806 ± 0.002	6.837 ± 0.002
	Volume (Å^3)	216.84 ± 0.01	-	217.03 ± 0.08	219.71 ± 0.08
c-NaBH$_4$	a (Å)	-	6.169 ± 0.002	6.163 ± 0.002	6.188 ± 0.001
	Volume (Å^3)	-	234.8 ± 0.013	234.06 ± 0.022	236.91 ± 0.11

Table B. 2 and Table B. 3 summarize the Raman and FTIR frequencies for the 0.91(0.62LiBH$_4$-0.38NaBH$_4$)-0.09Ni mixture compared with that for 0.62LiBH$_4$-0.38NaBH$_4$ mixture. As a metal, Ni was not detectable by vibrational techniques.

Table B. 2 Experimental wavenumbers (cm⁻¹) of the as-milled 0.91(0.62LiBH₄-0.38NaBH₄)-0.09Ni mixture observed in Raman compared with that for the as-milled 0.62LiBH₄-0.38NaBH₄

Mode		LiBH₄		NaBH₄		LiBH₄-NaBH₄	LiBH₄-LiBH₄-Ni
		As-milled	Lit. [B1-9]	As-milled	Lit. [B1-9]	As-milled	As-milled
v_4	A_g	1096	1097			1097	1097
v_4'	A_g	n.a.	1240			1242	1239
v_2	A_1			1277	1279	1282	1285
v_2	B_{1g}	1290	1290			1290	1291
v_2'	A_g	1319	1320			1317	1314
$2v_4$		2163	2157			2159	2156
$2v_4'$		2180	2177			2167	n.a.
$2v_4$				2195	2198	2198	2194
$2v_4$				2227	2229	2229	n.a.
v_3	A_g	2273	2275			2275	2273
v_1	A_g	2299	2299			2300	2298
v_1	A_1			2331	2335	2323	2324
v_2+v_4	E			2401	2403	2404	2399

Table B. 3 Experiment wavenumbers (cm⁻¹) of the as-milled 0.91(0.62LiBH₄-0.38NaBH₄)-0.09Ni mixture observed in FTIR compared as-milled 0.62LiBH₄-0.38NaBH₄

Mode		LiBH₄		NaBH₄		LiBH₄-NaBH₄	LiBH₄-LiBH₄-Ni
		As-received	Lit. [B9-10]	As-received	Lit. [B9-10]	As-milled	As-milled
v_4	A_g	1089	1089			1092	1092
v_4	B_2			1107	1119	1117	1116
v_4'	A_g	1233	1254			1237	1236
v_2	B_{1g}	1285	1284			1286	1286
v_2'	A_g	1307	1323			1310	1309
$2v_4'$		2180	2176			2180	2179
$2v_4$				2213	2222	2221	2222
v_3	A_g	2271	2277			2274	2275
v_3	B_2			2282	2297	2297	2295
v_3'	A_g	2300	2307				
v_2+v_4	E			2399	2393	2400	2400

Figure B. 2 shows the hydrogen desorption from the as-milled 0.91(0.62LiBH₄-0.38NaBH₄)-0.09Ni compared with the as-milled 0.62LiBH₄-0.38NaBH₄ mixture in the temperature range of 50 to 300 ℃. The onset dehydrogenation

temperature of 0.91(0.62LiBH$_4$-0.38NaBH$_4$)-0.09Ni locates in between 150 to 200 °C as a consequence of the small amount of NiO (1.3(3) wt.%).

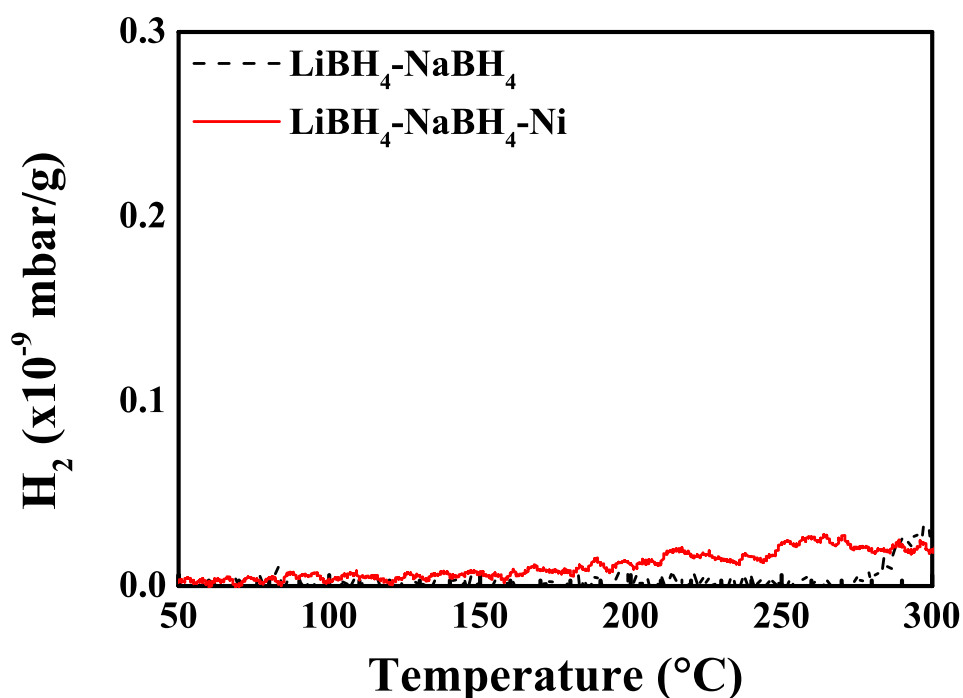**Figure B. 2 TPD-MS data show hydrogen desorption of the as-milled 0.91(0.62LiBH$_4$-0.38NaBH$_4$)-0.09Ni mixture, compared with that for the as-milled 0.62LiBH$_4$-0.38NaBH$_4$ mixture. Samples were heated at 2 °C min^{-1} in flowing Ar at 160 mL min^{-1} between 50 and 300 °C.**

Table B. 4 Summarizes the DSC curve areas for the as-milled 0.91(0.62LiBH$_4$-0.38NaBH$_4$)-0.09Ni compared with the as-milled 0.62LiBH$_4$-0.38NaBH$_4$ mixture. These area values are linearly proportional to the enthalpy.

Table B. 4 DSC curve areas for the as-milled 0.91(0.62LiBH$_4$-0.38NaBH$_4$)-0.09Ni mixture compared with that for the as-milled 0.62LiBH$_4$-0.38NaBH$_4$ mixture

	Sample	Energy			
		Heating		Cooling	
		Phase change	Fusion	Phase change	Solidification
		µV mg^{-1} LiBH$_4$	µV mg^{-1} LiNa	µV mg^{-1} LiBH$_4$	µV mg^{-1} LiNa
1	0.62LiBH$_4$-0.38NaBH$_4$	18.9 ± 1.0	12.7 ± 0.6	13.2 ± 0.7	12.8 ± 0.6
2	0.91(0.62LiBH$_4$-0.38NaBH$_4$)-0.09Ni	15.5 ± 0.7	11.1 ± 0.6	11.8 ± 0.6	10.4 ± 0.6

Figure B. 3 shows the room temperature Raman results of heat-treated 0.91(0.62LiBH$_4$-0.38NaBH$_4$)-0.09Ni samples (at 468 °C, 515 °C and 586 °C) compared with the as-milled LiNa-Ni mixture at room temperature. Due to high fluorescence effect, Raman data in the B-H stretching region are not available.
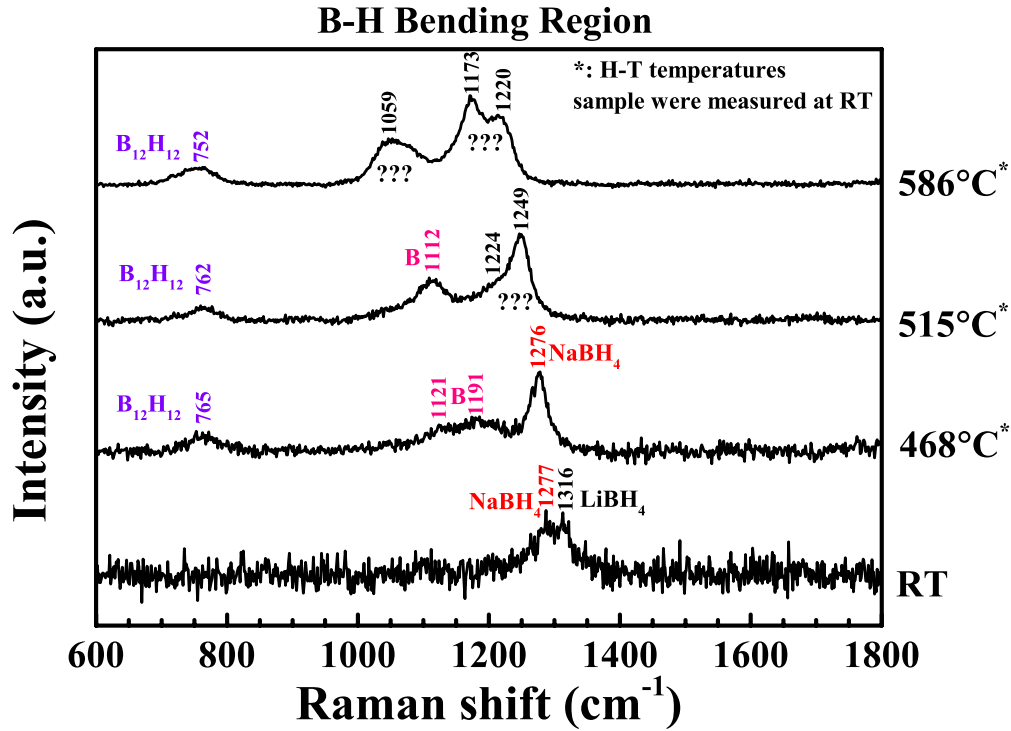

Figure B. 3 Room temperature Raman spectra of as-milled 0.91(0.62LiBH$_4$-0.38NaBH$_4$)-0.09Ni, which had been heat-treated at 468 °C, 515 °C and 586 °C in flowing Ar. The intensities of the Raman peaks were normalized.

Due to its high melting point, B (T$_{melt}$ = 2052.8 ± 21.3 °C) is expected to stay in solid-state once precipitated. Beside, since the Li$_2$B$_{12}$H$_{12}$ phase did not have any melting/fusion/frothing behavior when it is heated to 600 °C (thermogravimetric analysis, DTA/TGA) [B11], it is therefore expected in their solid-state in the decomposition products.

[B1]   Gomes S, Hagemann H, Yvon K. Lithium boro-hydride LiBH4. J Alloys Compd 2002;346:206–10. doi:10.1016/S0925-8388(02)00668-0.

[B2]   Hagemann H, Filinchuk Y, Chernyshov D, van Beek W. Lattice anharmonicity and structural evolution of LiBH4 : an insight from Raman and X-

ray diffraction experiments. Phase Transitions 2009;82:344–55. doi:10.1080/01411590802707688.

[B3] Reed D, Book D. In-situ Raman study of the thermal decomposition of LiBH4. MRS Proc 2009;1216. doi:10.1557/PROC-1216-W06-05.

[B4] Orimo SI, Nakamori Y, Ohba N, Miwa K, Aoki M, Towata SI, et al. Experimental studies on intermediate compound of LiBH4. Appl Phys Lett 2006;89:21920. doi:10.1063/1.2221880.

[B5] Gebert F, Willenberg B, Van Setten MJ, Bardají EG, Roehm E, Fichtner M, et al. Polarization-dependent Raman spectroscopy of LiBH4 single crystals and Mg(BH4)2 powders. J Raman Spectrosc 2011;42:1796–801. doi:10.1002/jrs.2934.

[B6] Racu A-M, Schoenes J, Lodziana Z, Borgschulte A, Züttel A. High-resolution Raman spectroscopy study of phonon modes in LiBH4 and LiBD4. J Phys Chem A 2008;112:9716–22. doi:10.1021/jp803005f.

[B7] Parker SF. Spectroscopy and bonding in ternary metal hydride complexes-Potential hydrogen storage media. Coord Chem Rev 2010;254:215–34. doi:10.1016/j.ccr.2009.06.016.

[B8] Harvey KB, McQuaker NR. Low Temperature Infrared and Raman Spectra of Lithium Borohydride. Can J Chem 1971;49:3282–6. doi:10.1139/v71-546.

[B9] Zavorotynska O, Corno M, Damin A, Spoto G, Ugliengo P, Baricco M. Vibrational properties of MBH4 and MBF4 crystals (M = Li, Na, K): A combined DFT, infrared, and Raman study. J Phys Chem C 2011;115:18890–900. doi:10.1021/jp2058244.

[B10] Harvey KB, McQuaker NR. Infrared and Raman Spectra of Potassium and Sodium Borohydride. Can J Chem 1971;49:3272–81. doi:10.1139/v71-545.

[B11] Pitt MP, Paskevicius M, Brown DH, Sheppard DA, Buckley CE. Thermal stability of Li2B12H12 and its role in the decomposition of LiBH4. J Am Chem Soc 2013;135:6930–41. doi:10.1021/ja400131b.

Appendix C Cycling stability of LiBH$_4$-NaBH$_4$ and LiBH$_4$-NaBH$_4$-Ni mixtures

Figure C. 1 shows the H$_2$ releases of each desorption process during cycling for the 0.62LiBH$_4$-0.38NaBH$_4$ and 0.91(0.62LiBH$_4$-0.38NaBH$_4$)-0.09Ni mixtures.
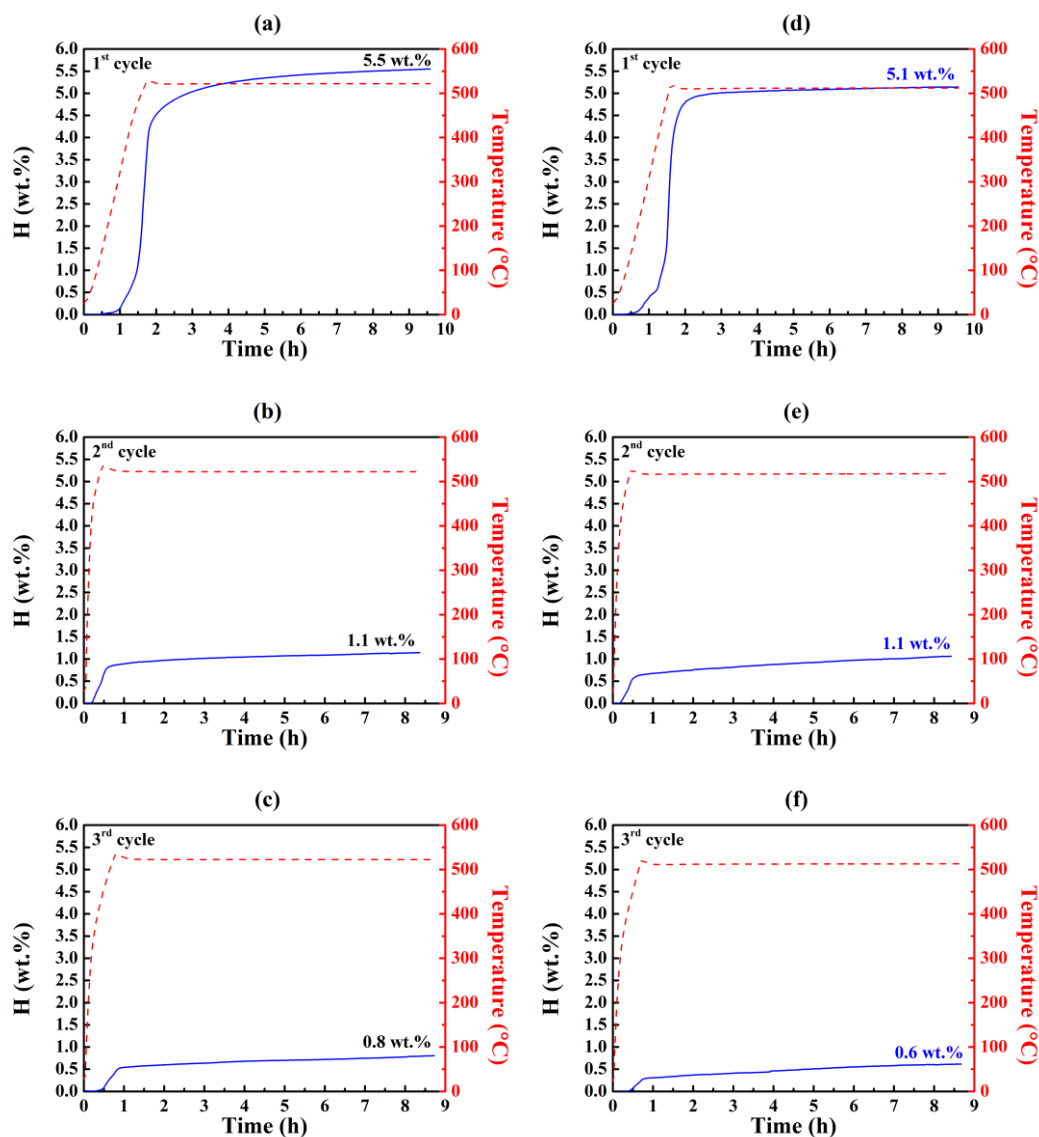

Figure C. 1 Sievert's measurements showing hydrogen release (in wt.%) while keeping the as-milled 0.62LiBH$_4$-0.38NaBH$_4$ (a, b, c) and 0.91(0.62LiBH$_4$-0.38NaBH$_4$)-0.09Ni (d, e, f) mixtures under 1 bar H$_2$ at 500 °C ($\Delta T/\Delta t$ = 5 °C min^{-1}) for 10 h for desorption and under 130 bar H$_2$ at 400 °C for 12 h for rehydrogenation.

Figure C. 2 and Figure C. 3 show the PXD and FTIR results for the 0.62LiBH$_4$-0.38NaBH$_4$ and 0.91(0.62LiBH$_4$-0.38NaBH$_4$)-0.09Ni mixtures during cycling. The Cu based impurities (Cu$_2$O and CuO) observed in PXD pattern was introduced

from the outer surface of sample holder during operation (not participated in dehydrogenation). No $[B_nH_n]^{2-}$ has been seen in PXD patterns (10-20° 2θ).
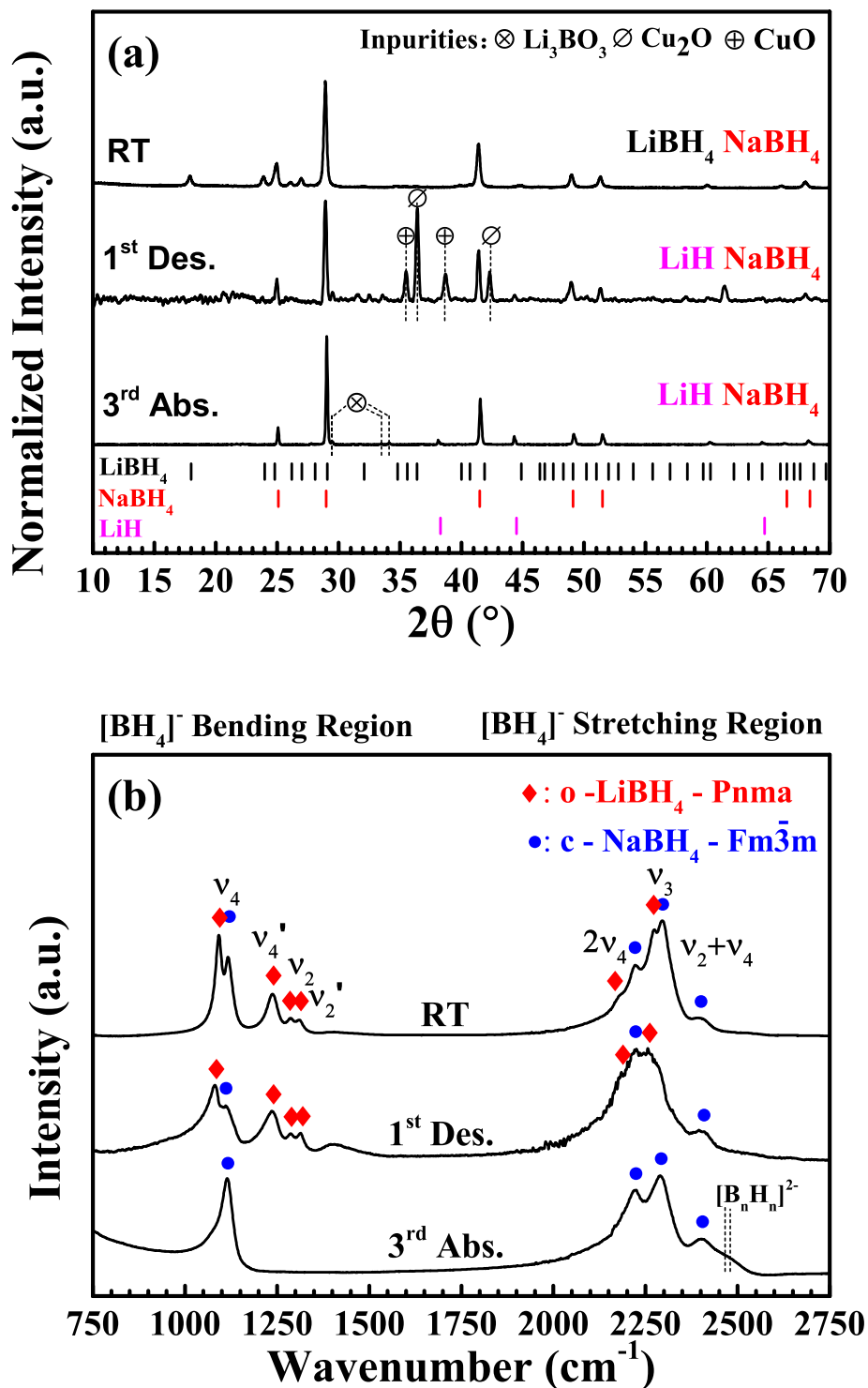

Figure C. 2 (a) PXD pattern (Cu Kα, λ = 1.5418 Å) and (b) FTIR spectrum of 0.62LiBH₄-0.38NaBH₄ decomposed at 500 °C in 1 bar static H₂ for 10 h (denoted as 1st Des.) and recombined in 130 bar H₂, 400 °C for 12 h at 3rd reabsorbed states (denoted as 3rd Abs.), compared with the as-milled sample (denoted as RT).
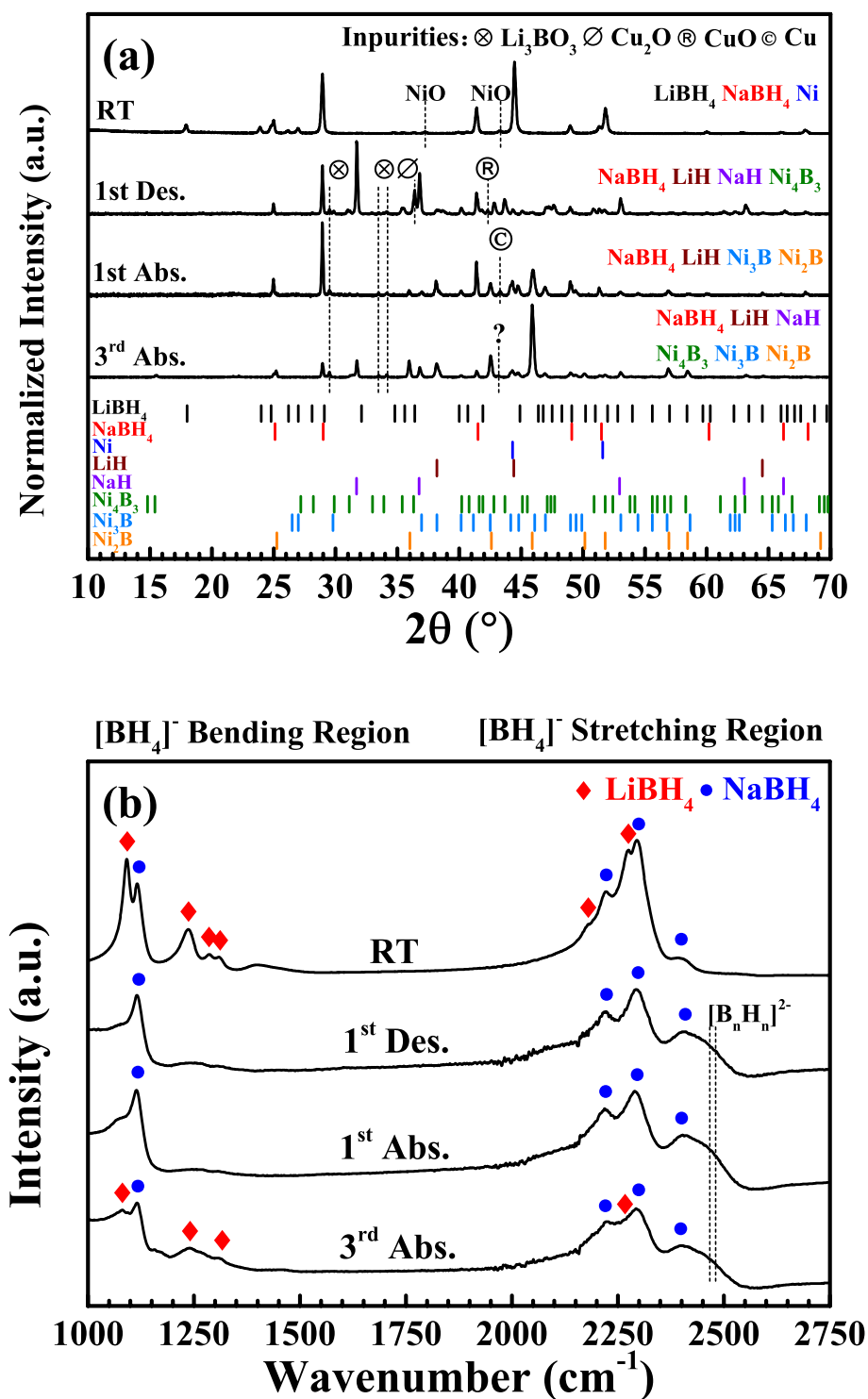
Figure C. 3 (a) PXD pattern (Cu K$_\alpha$, λ = 1.5418 Å) and **(b)** FTIR spectrum of 0.92(0.62LiBH$_4$-0.38NaBH$_4$)-0.09Ni decomposed at 500 °C in 1 bar static H$_2$ for 10 h (denoted as 1st Des.) and recombined in 130 bar H$_2$, 400 °C for 12 h at 1st and 3rd reabsorbed states (denoted as 1st Abs. and 3rd Abs., respectively), compared with the as-milled sample (denoted as RT).

Appendix D Dehydrogenation behavior of LiBH4-Ni system

To characterize the nano-sized effect of Ni addition, two types of Ni powder from Sigma-Aldrich (bulk: average mean size 3 μm, 99.7%; nano-sized: average mean size <100 nm, 99.9%) were mixed with $LiBH_4$ using ball milling. Figure D. 1 shows their temperature-dependent desorption results from 50 °C to 500 °C in flowing Ar using TPD-MS.
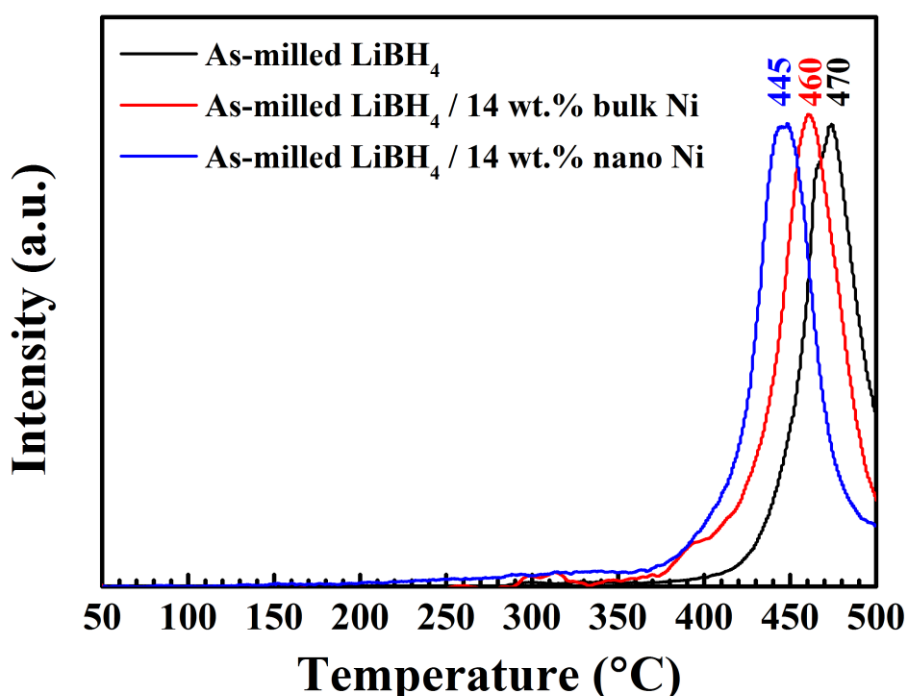

Figure D. 1 TPD-MS results of as-milled $LiBH_4$-Ni (14 wt.%) samples in the range of 50-500°C heated at 2 °C min^{-1} in contrast to as-milled $LiBH_4$. The desorbed H_2 was carried by Ar flowing at 160 mL min^{-1} and measured by MS. Signals were normalized for comparison. No B_2H_6 was detected.

The $LiBH_4$-Ni (bulk) sample started dehydrogenation at 287 °C that was very close to 285 °C for the as-milled $LiBH_4$. Thus, the added 14 wt.% bulk Ni did not decrease the decomposition onset temperature. However, it reduced the peak temperature by 10 °C (to 460 °C) compared with the 470 °C for the as-milled $LiBH_4$. Upon heating to 500 °C, the amount of H_2 released from the $LiBH_4$-Ni (bulk) sample was 5.2 wt.%. If the weight of Ni is excluded, $LiBH_4$ content released 6.0 wt.% of hydrogen, which was slightly smaller than the 6.7 wt.% for the as-milled $LiBH_4$.

The nano-sized Ni not only decreased the decomposition onset temperature (from 285 °C for as-milled LiBH$_4$) to 187 °C, but also reduced the peak temperature by 25 °C (to 445 °C) compared with the 470 °C for Ni-free sample. In contrast to the bulk Ni sample, this peak temperature was also 15 °C lower.

The decrease of onset temperature was possibly due to the NiO presented; whilst the reduction in peak temperature was caused by the nano-sized Ni additive and enhanced by its nano-scale effect when compared with the bulk Ni sample. The H$_2$ release from nano-sized Ni sample was 5.5 wt.% when heated to 500 °C. This value was close to the 5.2 wt.% for bulk Ni sample. They were about half of the 12.3 wt.% reported by Ref. [D1] for a LiBH$_4$-Ni (25 wt.%) sample when heated to 527 °C using a Thermo-Gravimetric Analysis (TGA) apparatus. Since this work used different experimental conditions (such as size and amount of nano-sized Ni, sample preparation methods, equipment and decomposition conditions) when compared with Ref. [D1], it is difficult to determine the reason for this difference in observed H$_2$ evolutions. Moreover, considering the available composition of LiBH$_4$ in the nano-sized Ni sample, about 6.4 wt.% of hydrogen was released from the LiBH$_4$ content, which was slightly larger than the 6.0 wt.% for the bulk Ni sample but was still smaller than the 6.7 wt.% for Ni-free sample.

[D1] Li H, Yan Y, Akiba E, Orimo S. Improved Dehydrogenation and Rehydrogenation Properties of LiBH4 by Nanosized Ni Addition. Mater Trans 2014;55:1134–7. doi:10.2320/matertrans.MG201407.